

Tesi doctoral presentada per En/Na

**Marc PERA TITUS**

amb el títol

**"Preparation, characterization and modeling of  
zeolite NaA membranes for the pervaporation  
dehydration of alcohol mixtures"**

per a l'obtenció del títol de Doctor/a en

QUÍMICA

Barcelona, 29 de maig del 2006

Facultat de Química  
Departament d'Enginyeria Química



UNIVERSITAT DE BARCELONA



Given the results shown in the precedent sections concerning the preparation of inner side tubular zeolite NaA membranes (chapter IV), the effect of the operational conditions on their performance (chapter V), the characterization of large defects in zeolite NaA layers (chapter VI), and the binary adsorption equilibrium of water and ethanol vapors in zeolite NaA powder (chapter VII), this chapter provides an insight into the mechanisms that govern the dehydration performance of zeolite NaA membranes in the PV process. To this end, the generalized Maxwell-Stefan theory (GMS) under the Langmuir formalism, traditionally applied for the description of gas permeation through MFI zeolite membranes, has been extended to PV to account for the selective water removal shown by hydrophilic zeolite membranes. It should be emphasized that, despite the limitations of the Langmuir formalism from a thermodynamic point of view according to the conclusions derived from the use of Potential Thermodynamic Isotherms (PTIs) (see section VI.2), this formalism will be used in the remainder of this section to account phenomenologically for mass transfer in zeolite NaA powder and zeolite NaA membranes.

Section VIII.1 includes the experimental results concerning the determination of Maxwell-Stefan (MS) surface diffusivities for water and ethanol vapors in zeolite NaA commercial powder from unary adsorption kinetics. Moreover, section VIII.2 shows the modeling of the PV process in zeolite NaA membranes prepared in our laboratory towards the dehydration of ethanol/water mixtures. Section VIII.2.1 shows a first approach into the subject by modeling the binary equilibrium adsorption in the zeolite NaA layers by means of the Extended Langmuir isotherm. Subsequently, the modeling is improved in section VIII.2.2 by using the PRAS theory to account for the binary equilibrium adsorption and by including the effect on meso- and macroporous defects. In both approaches, Maxwell-Stefan surface diffusivities for water and ethanol are derived from fittings of experimental PV data to the model. MS surface diffusivities of water are some orders of magnitude higher than the values that can be found from unary adsorption kinetics of water vapor in zeolite NaA powder, which might imply a possible effect of grain boundaries and surface barriers in the performance of the membranes, as will be discussed in section VIII.3.

### **VIII.1. DETERMINATION OF MS SURFACE DIFFUSIVITIES OF WATER AND ETHANOL VAPORS IN ZEOLITE NaA POWDER**

This section shows the unary adsorption kinetics of water vapor in zeolite NaA commercial powder from transient weight uptake in a microbalance (TGA) (see section VIII.1.2) and from breakthrough curves obtained in the differential packed bed (see section VIII.1.3). The experimental conditions explored to determine the adsorption kinetics of both species are the same as those surveyed for the determination of the adsorption isotherms (see

Table VI.2). Mass transfer from the outside to the inside of the particles can be regarded as an internal or *intracrystalline* mass transfer (IMT) process that might also show some contribution from external mass transfer (EMT). Accordingly, the contribution of the latter to the overall adsorption kinetics determined by both methods is first evaluated in section VIII.1.1

### VIII.1.1. External mass transfer (EMT)

In general terms, the resistance of a gas film or EMT can be reduced by increasing the velocity of the gas and by reducing the mean particle size. If the EMT is rate limiting, the flow of a generic species  $i$ ,  $N_i$  [ $\text{mol m}^{-2} \text{s}^{-1}$ ], can be described by Eq. VIII.1

$$N_i = k_G \frac{P_i}{RT}, \quad (\text{Eq. VIII.1})$$

where  $k_G$  is the EMT coefficient [ $\text{m s}^{-1}$ ] and  $P_i$  is the partial pressure of species  $i$  in the bulk of the gas phase [Pa]. The comparison of the flow of species  $i$  calculated by Eq. VIII.1 with the experimental values would determine whether this step is controlling or not. The contribution of the EMT to the overall mass transfer can be evaluated by means of the *Mears criterion* (Levenspiel, 1999). According to this criterion, the contribution of the EMT can be neglected if the following condition is fulfilled:

$$\frac{(P_{i,\text{bulk}} - P_{i,\text{surf}})}{P_{i,\text{bulk}}} = RT \frac{N_i}{k_{g,i} P_{i,\text{bulk}}} \leq 0.1 \quad (\text{Eq. VIII.2})$$

where  $P_{i,\text{bulk}}$  and  $P_{i,\text{surf}}$  are the partial pressures of species  $i$  in the bulk phase and on the surface of the particles [Pa], respectively. The EMT coefficients,  $k_{G,i}$ , for the special case of low particle Reynolds number values ( $0.01 < \text{Re}_p < 1000$ ) and high bed porosities ( $\epsilon_b > 0.60$ ), can be estimated by the *Nelson and Galloway method* (Doraiswamy and Sharma, 1984) (see Appendix E), which provides values in the range  $\text{cm s}^{-1}$ . For the special case of water vapor, the estimated values of the  $k_G$  coefficient for water vapor lie in the range  $0.78 - 1.20 \text{ cm s}^{-1}$  for the temperature range 305-423 K, which implies a maximum contribution of the EMT to the overall mass transfer  $< 0.01$  (1%) ( $T = 423 \text{ K}$ , total gas flow =  $200 \text{ cm}^3 \text{ (STP) min}^{-1}$ ;  $N_i(t=0) = 3.03 \times 10^{-7} \text{ mol m}^{-2} \text{ s}^{-1}$ ,  $P_{w,\text{bulk}} = 133 \text{ Pa}$ , and  $k_G = 1.20 \text{ cm s}^{-1}$ ). For the range of conditions surveyed in this work, the EMT does not appear to contribute to the adsorption kinetics of water vapor in zeolite NaA powder determined either in a microbalance and from breakthrough curve analysis.

Furthermore, in order to assess that the form of the weight uptake curves was not affected by the total gas flow, some preliminary experiments were carried out in the packed

bed for a total gas flow in the range  $50 - 200 \text{ cm}^3 \text{ (STP) min}^{-1}$  at 423 K and for a water partial pressure at the inlet of the packed bed in the range 1266 – 1533 Pa (see Figure VIII.1). As can be seen in Figure VIII.1, although the final value of water loading tends to the same value when working at different total flows, the adsorption curves do not seem to be affected by the total gas flow only beyond  $100 \text{ cm}^3 \text{ (STP) min}^{-1}$ , which confirms the conclusion derived from the *Mears Criterion* that the EMT is negligible for  $200 \text{ cm}^3 \text{ (STP) min}^{-1}$  total gas flow in the packed bed.

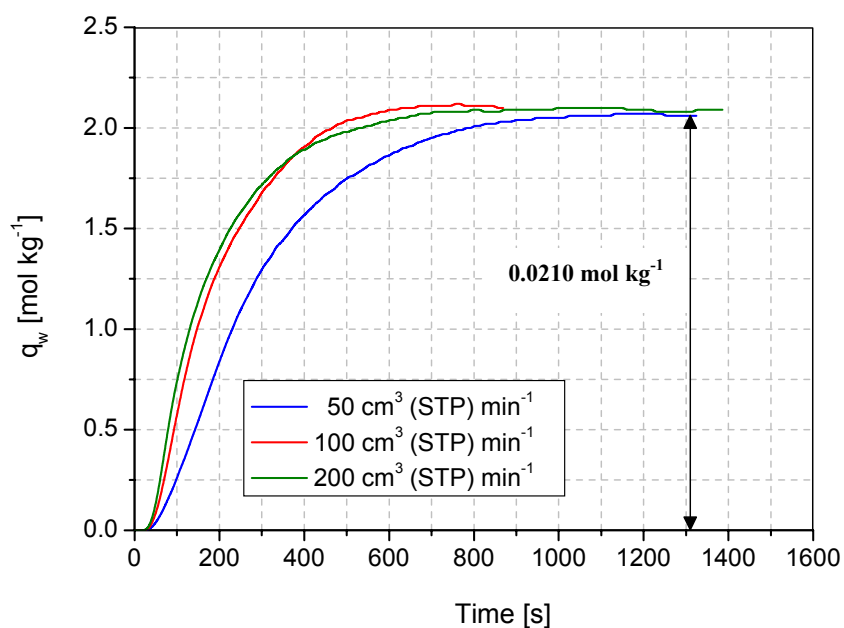


**Figure VIII.1:** Weight uptake curves of water obtained from breakthrough curve analysis at the outlet of the packed bed for the total gas flow range  $50 - 200 \text{ cm}^3 \text{ (STP) min}^{-1}$ . Experimental conditions:  $T = 423 \text{ K}$ ;  $p_w^{\text{in}} = 1266 - 1533 \text{ Pa}$ ;  $m_{\text{ZA}} = 100.7 \text{ mg}$ .

### VIII.1.2. Determination of MS surface diffusivities of water in zeolite NaA powder from weight uptake in a microbalance

MS surface diffusivities of water in zeolite NaA powder were determined from weight uptake in the microbalance after exposure to an atmosphere with a fixed water partial pressure. The experiments were carried out with small amounts of zeolite NaA powder compared to the total gas flow to assure differential conditions. The details concerning the experimental procedure to determine the adsorption kinetics in the microbalance can be found in section III.3.1.

Provided that the packed bed operates at differential conditions and neglecting the contribution or *intercrystalline* diffusion, the adsorption kinetics can be only accounted for by intracrystalline mass transfer by surface diffusion from the outside to the inside of the zeolite particles on the sample holder (see Figure III.18). Assuming that the particles are spherical according to the SEM images shown in Figure VII.3d., mass transfer can be described by a microscopic mass balance in spherical coordinates (Eq. VIII.3)

$$\frac{\partial \theta}{\partial t} = \frac{1}{r^2} \frac{\partial}{\partial r} \left[ r^2 \frac{\mathcal{D}^S(\theta)}{(1-\theta)} \frac{\partial \theta}{\partial r} \right], \quad (\text{Eq. VIII.3})$$

with the following set of boundary and initial conditions (Eqs. VIII.4-VIII.6)

Boundary conditions (BC):

$$1) \quad \forall t, r=0 \rightarrow \left. \frac{\partial \theta}{\partial r} \right|_{r=0} = 0 \quad (\text{Eq. VIII.4})$$

$$2) \quad \forall t, r=R \rightarrow \theta = \theta_{\text{eq}} \quad (\text{Eq. VIII.5})$$

Initial conditions (IC):

$$3) \quad \forall r \neq R, t=0 \rightarrow \theta = 0 \quad (\text{Eq. VIII.6})$$

$$r=R, t=0 \rightarrow \theta = \theta_{\text{eq}} = \theta_{\text{eq}}(P_i, T)$$

In Eqs. VIII.3-VIII.6,  $\theta$  is the fractional occupancy at each position of the particle ( $0 \leq \theta \leq 1$ ) [-],  $\theta_{\text{eq}}$  is the fractional occupancy at equilibrium given the temperature and partial pressure of species  $i$  in the experiment,  $R$  is the radius of the particle [m],  $r$  is the distance from the center of the particle ( $0 \leq r \leq R$ ),  $\mathcal{D}^S(\theta)$  is the MS surface diffusivity of the transferred species from the outside to the inside of the particle [ $\text{m}^2 \text{s}^{-1}$ ], and  $t$  is the elapsed time [s]. In this study, the following models for MS surface diffusivities were taken into account (see section I.3.7.3):

$$\text{Weak confinement:} \quad \mathcal{D}^S(\theta) = \frac{1}{Z} \lambda^2 v(\theta) = \mathcal{D}^S(0) \quad (\text{Eq. VIII.7})$$

$$\text{Strong confinement:} \quad \mathcal{D}^S(\theta) = \frac{1}{Z} \lambda^2 v(\theta) \quad \theta_v = \mathcal{D}^S(0)(1-\theta) \quad (\text{Eq. VIII.8})$$

which are regarded as temperature-dependent according to the Arrhenius equation analogous to Eq. I.40 (Eq. VIII.9)

$$\mathcal{D}(\theta)(T) = \mathcal{D}(\theta)(T_M) \exp \left[ -\frac{E_w^S}{R} \left( \frac{1}{T} - \frac{1}{T_M} \right) \right] \quad (\text{Eq. VIII.9})$$

where  $T_M$  is the mean temperature of the experimental series (363.4 K) and  $E_w^S$  is the activation energy for diffusion [ $\text{kJ mol}^{-1}$ ] through the window openings in the  $\alpha$ -cages (see Figure I.3). Furthermore, in the calculations, the mean loading of a particle of radius  $R$ ,  $\bar{\theta}$ , and the mean loading of a bed of particles of radius  $R$ ,  $\bar{\bar{\theta}}$  can be computed, respectively, by Eqs. VIII.10 and VIII.11

$$\bar{\theta} = \frac{\int_V \theta \delta V}{\int_V \delta V} = \frac{\int_0^R \theta 4\pi r^2 \delta r}{\frac{4}{3}\pi R^3} = \frac{3}{R^3} \int_0^R \theta r^2 \delta r \quad (\text{Eq. VIII.10})$$

$$\bar{\bar{\theta}} = \frac{\int_0^{+\infty} v(R) \bar{\theta} \delta V}{\int_0^{+\infty} v(R) \delta V} = \frac{\int_0^{+\infty} v(R) \bar{\theta} 4\pi R^2 \delta R}{\int_0^{+\infty} v(R) 4\pi R^2 \delta R} = \frac{\int_0^{+\infty} v(R) \bar{\theta} R^2 \delta R}{\int_0^{+\infty} v(R) R^2 \delta R} \quad (\text{Eq. VIII.11})$$

where  $R$  is the radius of a particle [m],  $v_j$  and  $\bar{\theta}_j$  are, respectively, the relative frequency [-] and the mean loading [-] of the particle of radius  $R$  according to Figure VII.2.

Using the set of boundary and initial conditions in Eqs VIII.4-VIII.6, Eqs. VIII.7 and VIII.8 for MS surface diffusivities, and Eqs. VIII.10 and VIII.11 for mean loadings, Eq. VIII.3 can be solved numerically through spatial and temporal discretization of a particle of radius  $R$  by the Crank-Nicholson method. A least-square non-linear optimization method based on the Levenberg-Marquardt algorithm was employed to adjust  $\mathcal{D}_w^S(0)$  parameters. The details concerning the resolution of Eq. VIII.3 and fitting to experimental adsorption uptake data to adjust  $\mathcal{D}_w^S(0)$  parameters for water can be found in Appendix F. The number of position intervals (50) and time intervals (10) was chosen to avoid any dependence of the optimized curves on them. The independence of the optimized values of the fitted parameters respect to their initial values was also checked.

Finally, it should be noted that, for the particular case of strong confinement and at differential conditions, the set of Eqs. VIII.3-VIII.6 and VIII.8 admits analytical solution. The one-species fractional occupancy is for this problem given by *Crank (2004)* (Eq. VIII.12)

$$\frac{\theta(t) - \theta(t_o)}{\theta(t_\infty) - \theta(t_o)} = 1 - \frac{6}{\pi^2} \sum_{m=1}^{\infty} \frac{1}{m^2} \exp\left[-m^2 \pi^2 \frac{\mathcal{D}^S(0)t}{R^2}\right] \quad (\text{Eq. VIII.12})$$

For short times, Eq. VIII.12 can be simplified to Eq. VIII.13, where it can be observed that the fractional occupancy is linear with the square root of time or Fourier number ( $Fo = \mathcal{D}(0)t/R^2$ )

$$\frac{\theta(t) - \theta(t_o)}{\theta(t_\infty) - \theta(t_o)} = \frac{6}{\pi^{1/2}} \left[ \frac{\mathcal{D}^S(0)t}{R^2} \right]^{1/2} = \frac{6}{\pi^{1/2}} (Fo)^{1/2} \quad (\text{Eq. VIII.13})$$

### VIII.1.3. Determination of MS surface diffusivities of water and ethanol from breakthrough curves obtained in a differential packed bed

MS surface diffusivities of water in zeolite NaA powder have been also determined experimentally from breakthrough curve analysis in a differential packed bed. The details concerning the experimental procedure to determine the adsorption kinetics from breakthrough curve analysis can be found in section III.3.2.

The general criteria outlined in section V.3.2.1 for fixed-bed reactor modeling have been used in this section to discard any phenomenon that might imply a deviation from the ideal plug flow model. According to *Rase (1977)*, the most relevant phenomena that might distort the hydrodynamics from the idealized plug flow are: (1) velocity gradients normal to the flow direction due to wall effects, (2) axial dispersion, (3) velocity gradients caused by a poor distribution of the species, (4) radial temperature and concentration gradients, and (5) channeling and shortcuts. For the packed bed used in this study, phenomena (1) – (4) can be neglected because the condition  $D_b/D_p = 3400 > 100$  and  $L_b/D_p = 4800 > 30$  are actually fulfilled. Furthermore, as was outlined in section V.3.2.1, the presence of very small zeolite particles can lead to local variations of porosity, which might cause channeling (5) in the bed. In the packed bed used in this study, channeling can be in principle ruled out, since some preliminary experiments carried out for water vapor adsorption at the same conditions (temperature, water vapor pressure at the inlet of the bed, and zeolite NaA weight) but changing the solid sample showed good reproducibility. Therefore, according to the general comments aforementioned, the hydrodynamics of the packed bed under study can be approached to the idealized plug flow.

For the special case of plug flow and at differential conditions, the adsorption kinetics can be only accounted for by intracrystalline mass transfer by surface diffusion from the outside to the inside of the zeolite particles in the packed bed, in the same way as that exposed for the particles on the sample holder in the experiments carried out in the microbalance (see section VIII.1.2). Assuming again that the particles are spherical, mass transfer can be described by the same set of Eqs. VIII.3-VIII.14 and solved following the recipe provided in section VIII.1.2. In addition, to check that the bed actually operated at differential conditions, some preliminary calculations were performed to discard the effect of the axial coordinate in the fittings. For such calculations, at pseudo-steady-state, the differential Eq. VIII.14 was included to the set of Eqs. VIII.3-VIII.8

$$\frac{w^T}{P_T} \frac{\delta P_i}{\delta W} = -N_i \Big|_{r=R} S_{\text{ext}} \quad , \quad (\text{Eq. VIII.14})$$

where  $\mathbf{w}^T$  is the total flow in the bed [ $\text{mol s}^{-1}$ ],  $\mathbf{W}$  is the weight of zeolite NaA powder in the bed [g],  $\mathbf{P}_i$  is the partial pressure of species  $i$ ,  $\mathbf{P}_T$  is the total pressure,  $\mathbf{S}_{\text{ext}}$  is the geometrical external surface of the particles ( $1.37 \text{ m}^2 \text{ g}^{-1}$ ), and  $\mathbf{N}_i|_{r=R}$  is the surface flow at the external surface of the particles [ $\text{mol m}^{-2} \text{ s}^{-1}$ ]. Eq. VIII.14 was solved numerically by approximating derivatives to finite differences for a particular number of axial position intervals in the bed,  $N$  [-], thus finally obtaining Eq. VIII.15

$$\frac{(P_i^{k+1} - P_i^k)}{\Delta W} = N_i|_{r=R} S_{\text{ext}} \frac{P_T}{W^T}, \quad (\text{Eq. VIII.15})$$

where  $k = 1, \dots, N$  and  $\Delta W = m_{ZA}/N$ . For the tested experimental conditions, the packed bed was checked to behave at differential conditions, since the optimized values of the fitted MS surface diffusivities at zero coverage were found not to depend on the number of position intervals in the range  $N=0-20$ .

#### VIII.1.4. Fitting of experimental adsorption kinetic data of water and ethanol vapors to the model

Some examples of the fittings of the model to experimental weight uptake curves of water vapor obtained from breakthrough curve analysis at the outlet of the differential packed bed for weak confinement are plotted in Figure VIII.2. On the basis that the fittings are uniparametric, namely **only one parameter** is fitted, the fittings reproduce successfully the experimental weight uptake curves of water, especially for temperatures  $>363 \text{ K}$ . The confidence interval of the fitted MS surface diffusivities at zero coverage was found to be the lowest for all the curves obtained at temperatures  $>363 \text{ K}$  ( $<13\%$  for a confidence interval for a probability level of 95%), while between 15-40% for the curves obtained at 305 and 333 K. Furthermore, it should be noted that the values found from the numerical resolution of Eq. VIII.3 for the situation of strong confinement are in agreement with those determined by Eq. VIII.13 for short times.

On the other hand, although no significant differences were found in terms of calculated sum of squares (SQs) when fitting the model to experimental data for both weak and strong confinement (models I and II, respectively), the values of MS surface diffusivities at zero coverage for weak confinement (Eq. VIII.7) are practically independent of the water partial pressure at the inlet of the packed bed or in the holder of the microbalance (see Figure VIII.3), while a higher dispersion of the values is observed for strong confined MS surface diffusivities at zero coverage (Eq. VIII.8). Moreover, the fitted MS surface diffusivities at zero coverage for weak and strong confinement are in their turn fitted to Eq. VIII.9 to account for their evolution with temperature (see Figure VIII.4). The following trends are obtained:



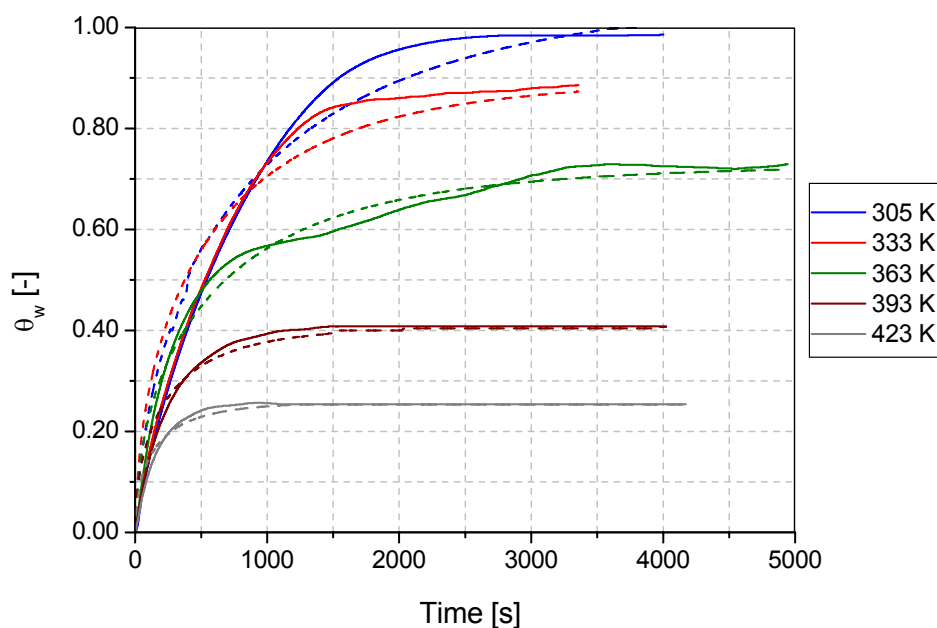


**Figure VIII.2:** Experimental and fitted trends for water uptake obtained from breakthrough curves of water vapor at the outlet of the differential packed bed for the temperature range 305-423 K. Experimental conditions: total gas flow = 200 cm<sup>3</sup> (STP) min<sup>-1</sup>; P<sub>w</sub><sup>in</sup> = 2100 Pa.

$$\text{Weak confinement: } \mathfrak{D}(0)(T) = (1.94 \pm 0.15)10^{-16} \exp\left[-\frac{(34 \pm 2)1000}{R}\left(\frac{1}{T} - \frac{1}{363.4}\right)\right]$$

$$\text{Strong confinement: } \mathfrak{D}(0)(T) = (3.61 \pm 0.69)10^{-16} \exp\left[-\frac{(20 \pm 5)1000}{R}\left(\frac{1}{T} - \frac{1}{363.4}\right)\right]$$

(Eqs. VIII.16 and VIII.17)

It should be noted that weak confined MS surface diffusivities provide lower confidence intervals (calculated on the basis of the fittings of the data plotted in Figure VIII.3 to Eqs. VIII.7 and VIII.8) for both the fitted activation energies and MS surface diffusivities at zero coverage at T<sub>M</sub> = 363.4 K, which reinforces the idea that the former diffusivities account for the diffusion of water in the zeolite NaA framework.

Finally, some preliminary determinations of MS surface diffusivities of ethanol in zeolite NaA powder at 423 K obtained from breakthrough curve analysis revealed a mean value of (5.99 ± 1.41) × 10<sup>-16</sup> m<sup>2</sup> s<sup>-1</sup> for low confinement. This value is ca. the half of that of

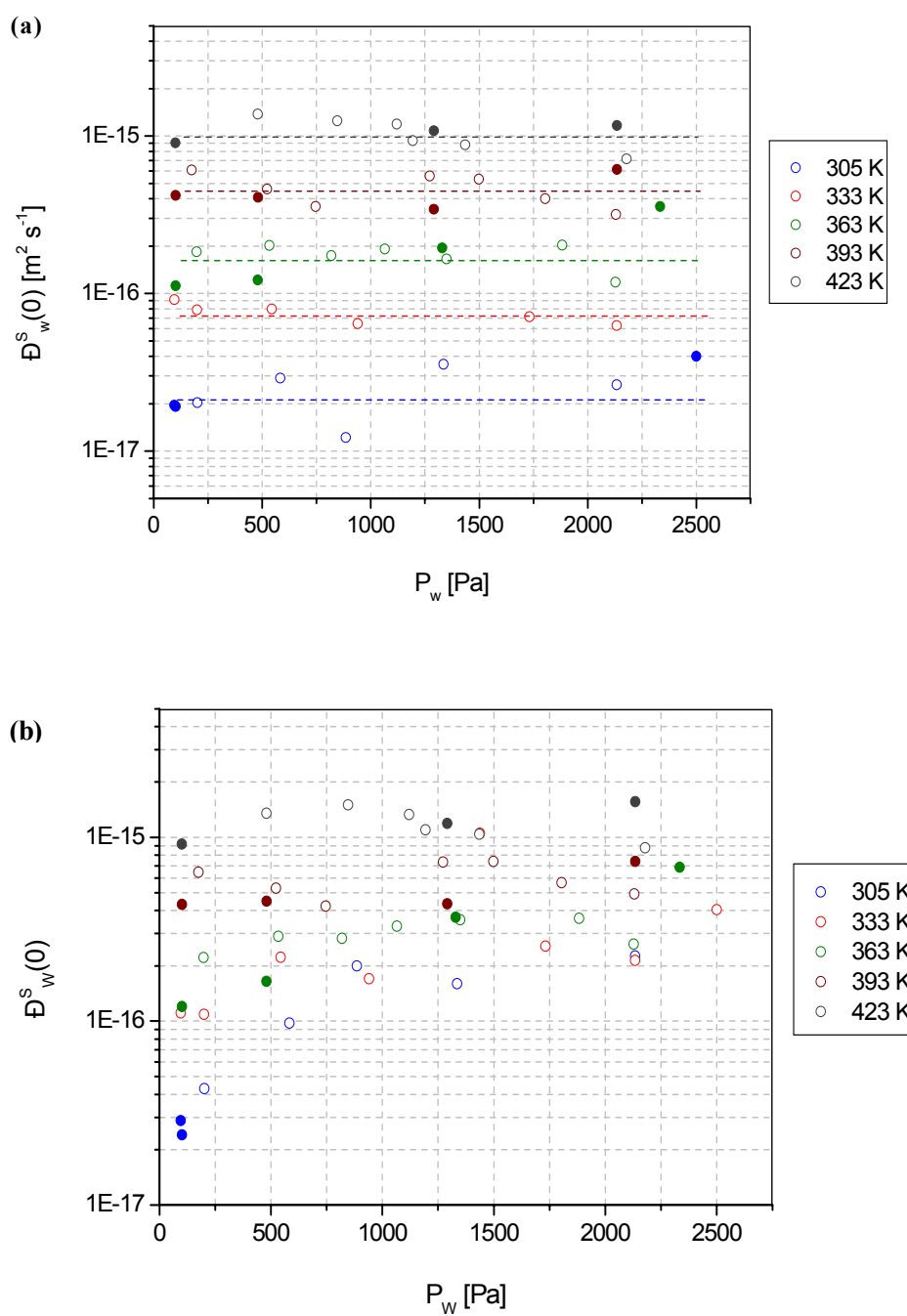


**Figure VIII.3:** Evolution of fitted MS surface diffusivities at zero coverage obtained from breakthrough curve analysis at the outlet of the packed bed (open cycles) and from weight uptake in the microbalance (closed cycles) for (a) weak confinement, and (b) strong confinement. Experimental conditions as in Table VII.2. Confidence interval <13% for T=363-423 K and in the range 15-40% for T=305-333 K.

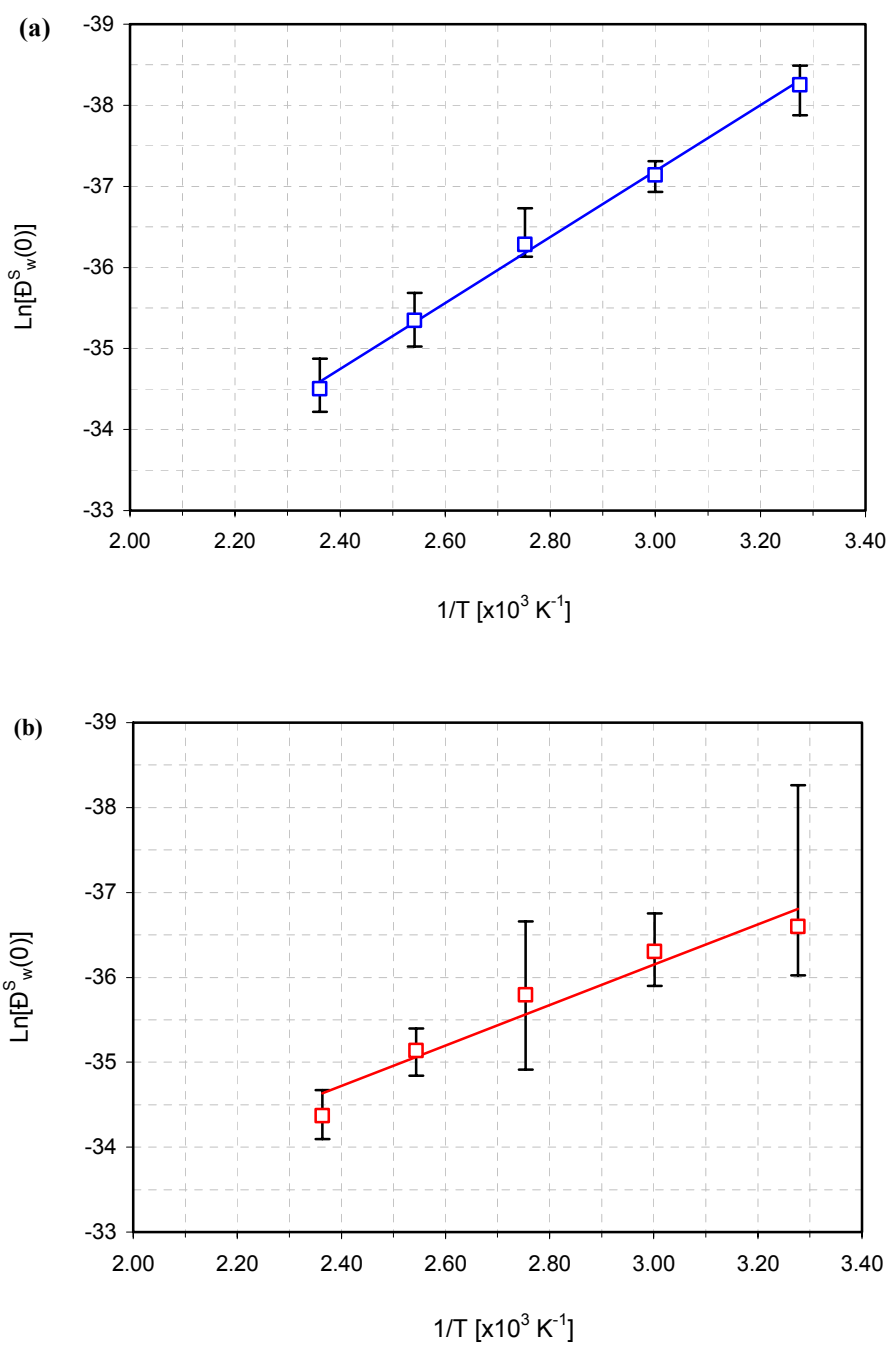


**Figure VIII.4:** Trend of fitted MS surface diffusivities at zero coverage with temperature for (a) weak confinement and (b) strong confinement. The confidence intervals are referred to dispersion of values shown in Figure VIII.3.

water determined at the same temperature. This result is consistent with the differences in the kinetic diameters of both molecules (0.29 vs. 0.43 nm, respectively) and the fact that the latter approaches the value of the pore of the window openings in the  $\alpha$ -cages of the LTA framework.

#### VIII.1.5. Comparison with literature data

Table VIII.1 summarizes the results obtained in section VIII.1.4 concerning the MS surface diffusivity values in zeolite NaA powder determined for both water and ethanol together with some transport and self-diffusivities of gases and vapors in zeolites reported in the literature. As can be seen, the MS surface diffusivities of water in zeolite NaA powder are of the same order of magnitude as transport diffusivities of H<sub>2</sub> in the same solid, a molecule with the same kinetic diameter as that of water (0.29 nm). Furthermore, the diffusivities for ethanol in zeolite NaA also shows the same order as those reported by *Nayak and Moffat (1988)* for the same species in MFI-type zeolites.

However, although MS surface diffusivities should in principle approach the values of self-diffusivities in light of the general comments exposed in section I.3.7.4, the experimental values of MS surface diffusivities at zero coverage determined from adsorption kinetics in this study for both water and ethanol are ca. 5 orders of magnitude lower than the self-diffusivities determined by *Paoli et al. (2002)* on zeolite NaA by the QENS and PFG-NMR techniques. It should be stressed that, according to *Gardner et al. (2002)*, these microscopic techniques tend to overestimate self-diffusivities, because equilibrium is seldom achieved and due to the influence of crystal edges and grain boundaries in their actual performance.

### VIII.2. MODELING MASS TRANSFER THROUGH ZEOLITE NaA MEMBRANES IN THE VPV PROCESS

This section is devoted to modeling the steady-state VPV performance of zeolite NaA membranes towards the dehydration of ethanol/water mixtures by means of the generalized Maxwell-Stefan (GMS) diffusional theory. In the present description, following the ideas put forward in section VI.2 and illustrated in Figure VI.1, composite zeolite NaA membranes are visualized as an assembly of zeolite grains that might include both *intracrystalline* or zeolite pores, and *intercrystalline* or non-zeolite pores related to grain boundaries between adjacent zeolite single crystals. In the present description, mass transfer through both kinds of pores is modeled as a global ensemble. Moreover, the presence of large meso- and macroporous defects (“*intercrystalline porosity*”) in the zeolite layers cannot be ruled out.

**Table VIII.1:** Surface diffusivities at zero coverage of water in zeolite NaA and comparison with literature data

<i>Zeolite</i>	<i>Species</i>	<i>Diffusivity values [m<sup>2</sup> s<sup>-1</sup>]</i>	<i>Technique</i>	<i>References</i>
Zeolite A	Water	3.9-7.9 × 10 <sup>-10</sup> (a,1) 10 <sup>-9</sup> - 10 <sup>-10</sup> (a,1) 3.0-5.0 × 10 <sup>-12</sup> (c,1) (1.06 ± 0.34) × 10 <sup>-15</sup> (c,2)	OBMC simulation <sup>(3)</sup> QENS / PFG RMN <sup>(4)</sup> VPV in a membrane Breakthrough curve Pure vapor uptake	Furukawa et al. (2004) Paoli et al. (2002) Shah et al. (2000) <b>This study</b>
	Ethanol	(5.99 ± 1.41) × 10 <sup>-16</sup> (c,2)	Breakthrough curve	<b>This study</b>
	1-hexane	2.0 × 10 <sup>-14</sup> (a,2) 2.5 × 10 <sup>-13</sup> (a,2)	PFG RMN NSE <sup>(5)</sup>	Jobic et al. (2003)
	H <sub>2</sub>	1.5 × 10 <sup>-15</sup> (b,1)	Pure vapor uptake	Breck (1984)
Zeolite Y	1-hexane	1.1 × 10 <sup>-15</sup> (b,2)	Pure vapor uptake	Masuda et al. (1996)
Zeolite MFI	Water	1.7 × 10 <sup>-9</sup> (a,1) 3.3 × 10 <sup>-9</sup> (a,1)	PFG-NMR MD	Bussai et al. (2002a)
	Methanol	5.7 × 10 <sup>-14</sup> (b,1)	Pure vapor uptake	Nayak and Moffat (1988)
	Ethanol	1.3 × 10 <sup>-14</sup> (b,1)		
	1-propanol	5.9 × 10 <sup>-15</sup> (b,1)		
	1-butanol	4.5 × 10 <sup>-15</sup> (b,1)		

(a) Self-diffusivity at zero coverage

(b) Transport diffusivity at saturation

(c) MS diffusivity at zero coverage

<sup>(1)</sup> Determined at 298-333 K<sup>(2)</sup> Determined at 423 K<sup>(3)</sup> OBMC: Orientational-Bias Monte Carlo<sup>(4)</sup> QENS: Quasi-elastic neutron scattering  
PFG RMN: Pulse field gradient NMR<sup>(5)</sup> NSE: Neutron spin-echo

In the present study, a set of steady-state VPV experiments performed with inner-side tubular zeolite NaA membranes synthesized in our laboratory (membranes ZA1-ZA3, see Table VIII.2) towards the dehydration of ethanol/water mixtures was used to model the PV process. The details concerning the preparation of the membranes and the range of values of the operational conditions tested are summarized, respectively, in Tables V.1 and V.2. The membranes consisted of a continuous active layer (thickness: 7-30 μm) of randomly oriented and intergrown zeolite NaA crystals located on the inner surface of porous α-alumina tubular supports. The zeolite NaA layers were grown by seeded hydrothermal synthesis (secondary-growth method) using the experimental procedures described in chapter IV. All the membranes displayed low N<sub>2</sub> permeances (<10<sup>-7</sup> mol m<sup>-2</sup> s<sup>-1</sup> Pa<sup>-1</sup>) and good PV performance for the separation of a 91.1 : 9.9 wt.% ethanol/water mixture at 323 K and with a permeate pressure kept <2 mbar. Moreover, the membranes showed a low amount of defects of mean

size in the range 3.5-15.9 nm and intercrystalline porosities in the range  $1.4 \times 10^{-5} - 2 \times 10^{-4}$  [-] according to the characterization method presented in section VI.2. The relevant structural parameters used in the modeling are listed in Table VIII.2.

**Table VIII.2:** Zeolite NaA membranes used in the present study. PV test:  $X_w = 6.67$ -9.92 wt.% ( $x_w = 0.15$ -0.22 mol%);  $T = 323$  K;  $P_o = 1$ -3 bar (100-300 kPa);  $P_v = 1$ -3 mbar (100-300 Pa)

Membrane	Code (see Table IV.3)	$\alpha_{w/E}$ [-]	$N^T$ [kg m <sup>-2</sup> h <sup>-1</sup> ]	$\ell_{ZA}$ [ $\mu$ m] <sup>1</sup>	Large defects <sup>2</sup>	
					$\bar{d}_c$ [nm]	$\epsilon_{inter} \times 10^4$ [-]
ZA1	ZA-INN-CF-03	294	0.39	30	9.7 ± 3.0	2.0 ± 1.0
ZA2	ZA-INN-SC-18	1050	0.49	35	15.9 ± 7.1	0.76 ± 0.2
ZA3	ZA-INN-C-05	8538	0.83	7	3.5 ± 1.6	0.14 ± 0.07

<sup>1</sup> Determined by SEM

<sup>2</sup> Determined by the characterization method presented in section VI.2

The experimental trends for both total flux,  $N^T$  [kg m<sup>-2</sup> h<sup>-1</sup>], and selectivity towards water removal,  $\alpha_{w/E}$  [-], with the feed composition, temperature, permeate pressure and retentate pressure for the dehydration of ethanol/water liquid mixtures by VPV with membranes ZA1-ZA3 have been shown in Figures V.1-V.6 (see section V.1) for the range of operational conditions listed in Table VIII.3 (Table V.2). In general terms, the dehydration of organic mixtures by VPV with zeolite NaA membranes is a temperature-dependent process with effective activation energy for water in the range 30-40 kJ mol<sup>-1</sup>. Furthermore, this process is also characterized by an increase of water flux with water feed composition until an asymptotic constant value beyond 30-40 mol% water (20-30 wt.%).

**Table VIII.3:** Experimental conditions for VPV experiments with ethanol/water mixtures

Feed flow rate [mL min <sup>-1</sup> ]	300
Water feed composition ( $X_w$ ) [wt.%]	1-60
Temperature (T) [K]	303-363
Stabilization time [h]	2-4
Experimental time [h]	1-3
Number of replicates [-]	2-6

### VIII.2.1. Mass transfer of adsorbed molecules by surface diffusion: Maxwell-Stefan diffusional theory

The general form of the GMS equations applied to surface diffusion in microporous materials that accounts for mass transfer through both zeolite and non-zeolite pores is given by Eq. VIII.18 (or I.35)

$$-\rho_p \frac{q_i}{RT} \nabla_T \mu_i = \sum_{\substack{j=1 \\ j \neq i}}^C \frac{(q_j N_i^S - q_i N_j^S)}{q_{M,j} \mathcal{D}_{ij}^S} + \frac{N_i^S}{\mathcal{D}_i^S} \quad i,j = 1,2,\dots, C \quad (\text{Eq. VIII.18})$$

where  $\nabla_T \mu_i$  is the isothermal surface chemical potential gradient of species  $i$ ,  $q_i$  and  $q_j$  are the loading of species  $i$  and  $j$  [-], respectively, and  $N_i^S$  and  $N_j^S$  are the surface fluxes of species  $i$  and  $j$  [mol m<sup>-2</sup> s<sup>-1</sup>], respectively. In the present description, the MS surface diffusivity is regarded to include the contributions of both zeolite pores and grain boundaries. As was aforementioned in section I.3.7.2, for cage-type zeolite topologies (3D) with high connectivities (e.g., LTA), the counterexchange coefficient  $\mathcal{D}_{ij}^S$  can be expected to be high (i.e.  $\mathcal{D}_{ij}^S \rightarrow \infty$ ), which implies that the mobility of adsorbed species  $i$  is not expected to contribute to the mobility of  $j$ . For this particular situation, the first term on the right-hand in Eq. VIII.18 vanishes and it transforms into Eq. VIII.19

$$N_i^S = -\rho_p \frac{q_i}{RT} \mathcal{D}_i^S \nabla_T \mu_i \quad i = 1,2,\dots, C \quad (\text{Eq. VIII.19})$$

Furthermore, Eqs. VIII.18 and VIII.19 allow to transform the surface chemical potential gradients into molar loading gradients as follows

$$\frac{q_i}{RT} \nabla_T \mu_i = \sum_{j=1}^N \Gamma_{ij} \frac{q_{i,M}}{q_{j,M}} \nabla q_j \quad \text{where } \Gamma_{ij} \equiv q_i \left( \frac{q_{j,M}}{q_{i,M}} \right) \frac{\partial \text{Ln}(P_i)}{\partial q_j} \quad i,j = 1,2,\dots, C$$

(Eqs. VIII.20 and VIII.21)

Using the definitions in Eqs. VIII.20 and VIII.21, Eq. VIII.19 transforms into Eq. VIII.22

$$N_i^S = -\rho_p \mathcal{D}_i^S \sum_{j=1}^N \Gamma_{ij} \frac{q_{i,M}}{q_{j,M}} \nabla q_j = -\rho_p \mathcal{D}_i^S \sum_{j=1}^N \frac{q_i}{P_i} \frac{\partial P_i}{\partial q_j} \nabla q_j \quad [\text{mol m}^{-2} \text{ s}^{-1}] \quad (\text{Eq. VIII.22})$$

Eq. VIII.22 constitutes the essential equation used in this section to model mass transfer through zeolite NaA layers in the VPV process for the dehydration of ethanol/water mixtures in the absence of contribution of counterexchange mobility of the adsorbed molecules. A next step in the present description involves the selection of a suitable multicomponent adsorption isotherm to determine the form of the thermodynamic factors,  $\Gamma_{ij}$ . In this study, for the VPV of

ethanol/water mixtures, both the Extended Langmuir (section VIII.2.2) and the PRAS formalisms (section VIII.2.3) have been used to account for the binary adsorption equilibrium of water and ethanol on the membrane, which allow the determination of Maxwell-Stefan surface diffusivities for both species,  $\mathbf{D}_w^S$  and  $\mathbf{D}_E^S$ , respectively.

In addition to Eq. VIII.22, because zeolite NaA membranes are grown onto a porous support, the contribution of the latter to the overall mass transfer in the VPV process should be in principle taken into account. Because the permeate is kept under vacuum in the VPV experiments, mass transfer through the macropores of the support in zone III can be assumed to occur by Knudsen diffusion. Therefore, the contribution of the support to the overall mass transfer can be evaluated by Eq. VIII.23 (or VI.64)

$$N_{III}^{Kn} = \sum_{i=1}^N \frac{D_{Kn,i}}{RT} \frac{(P_{v,i}^S - P_{v,i})}{\ell_s} = \sum_{i=1}^N \frac{\varepsilon_s \bar{d}_s}{3\tau_s RT} \sqrt{\frac{8RT}{\pi M_i}} \frac{(P_{v,i}^S - P_{v,i})}{\ell_s} \quad [\text{mol m}^{-2} \text{s}^{-1}], \quad (\text{Eq. VIII.23})$$

where  $\varepsilon_s$ ,  $\tau_s$ ,  $\ell_s$  and  $\bar{d}_s$  are, respectively, the porosity [-], tortuosity [-], thickness [m] and mean pore size of the support [m]. Moreover,  $P_{v,i}^S$  and  $P_{v,i}$  correspond, respectively, to the partial pressure [kPa] of the species  $i$  at the zeolite layer – support surface and in the bulk vapor permeate. For further details see section VI.2.1.3.

Finally, the contribution of large meso- and macroporous defects (“*intercrystalline porosity*”) to the overall mass transfer can be taken into account by using the characterization method presented in section VI.2. It should be noted that this contribution is relevant for the species with lower affinity for the zeolite material (i.e. ethanol in our case), especially for higher concentrations in the liquid feed.

## VIII.2.2. Preliminary modeling: Extended Langmuir approach

### VIII.2.2.1. Equations for water and ethanol fluxes

Although the Extended Langmuir isotherm (Eq. I.29) constitutes the simplest mathematical function to account for mixture adsorption, it only shows thermodynamic consistency if the adsorbing species have the same molar saturation loadings. As was outlined in section VII.1.3.2, water and ethanol do not actually show equal molar saturation loadings for their unary adsorption equilibrium in zeolite A, which implies that the binary adsorption equilibrium of both species is strongly governed by size entropy effects. Therefore, the Extended Langmuir isotherm does not appear to be appropriate for the description of the binary adsorption equilibrium of both species in zeolite A.



Nevertheless, in a first approach and for practical purposes, in light of the results presented in section VII.1.3, because zeolite NaA membranes pervaporate water selectively, the Extended Langmuir isotherm is used to account for the binary adsorption equilibrium of both species. Although the thermodynamic requirement of equal molar saturation loadings for each adsorbing species is not actually satisfied (11.4 vs. 3.5 mol kg<sup>-1</sup> for water and ethanol, respectively, see section VII.1.3.2), in order to be thermodynamically consistent, a constant saturation loading has been assumed (i.e.  $q_{M,w} = q_{M,E} = q_M$ , with mean value  $\sim 10$  mol kg<sup>-1</sup>) for competitive adsorption of water and ethanol. Despite the loss of scrupulosity, this assumption allows mathematical simplification of the binary diffusion process and to derive an analytical solution for the equations of diffusion (Eq. VIII.17), which reveals useful for practical applications and allows a direct comparison with the *solution-diffusion* model, widely used for modeling the PV process in polymeric membranes (see section I.4.3.2).

Furthermore, under the additional assumptions that (1) mass transfer of water and ethanol through a zeolite NaA layer (both through zeolite and non-zeolite pores) is the rate limiting step, and (2) water is preferentially adsorbed in the zeolite cavities compared to ethanol (i.e.  $q_w \gg q_E$ ) on the grounds of the hydrophilic character of zeolite NaA, Eq. VIII.19 is transformed into Eq. VIII.24 and VIII.25, respectively, for water and ethanol

$$N_w^S = -\rho_s q_M M_w \mathcal{D}_w^S(\theta_v) \frac{\nabla \theta_w}{(1 - \theta_w)} \quad [\text{kg m}^{-2} \text{s}^{-1}] \quad (\text{Eq. VIII.24})$$

$$N_E^S = -\rho_s q_M M_E \mathcal{D}_E^S(\theta_v) \left[ \nabla \theta_E + \theta_E \frac{\nabla \theta_w}{(1 - \theta_w)} \right] [\text{kg m}^{-2} \text{s}^{-1}], \quad (\text{Eq. VIII.25})$$

where  $\theta_w$  and  $\theta_E$  are the fractional occupancies of water and ethanol, respectively, on the zeolite layer. Moreover, assuming that mass transfer only takes place along the  $z$ -direction perpendicular to the membrane plane and that zeolite and non-zeolite pores are non-tortuous under the boundary conditions

$$z=0, \quad \rightarrow \quad \theta_w = \theta_{w,L}, \quad \theta_E = \theta_{E,L}$$

$$z = \ell_{ZA} \rightarrow \quad \theta_w = \theta_{w,v}, \quad \theta_E = \theta_{E,v}$$

The set of Eqs. VIII.24 and VIII.25 are solved analytically in sections VIII.2.2.2 and VIII.2.2.3, respectively, for both weak and strong confined MS surface diffusivities, through the convenient definition of dimensionless water and ethanol surface fluxes,  $\alpha_w$  and  $\alpha_E$ , respectively, which are defined by Eqs. VIII.26 and VIII.27

$$\alpha_w = \frac{N_w^S \ell_{ZA}}{\rho_s q_M M_w \mathcal{D}_w^S(0)} \quad [-] \quad \text{and} \quad \alpha_E = \frac{N_E^S \ell_{ZA}}{\rho_s q_M M_E \mathcal{D}_E^S(0)} \quad [-] \quad (\text{Eqs. VIII.26 and VIII.27})$$

In addition, water and ethanol loadings at both feed/ and permeate/membrane surfaces can be translated into partial pressures using the Extended Langmuir isotherm, where partial pressures at the former surface are assumed to be at equilibrium with the liquid mixture according to Eqs. VIII.28 and VIII.29

$$P_{w,L} = \gamma_w(x_{w,L}, T)x_{w,L} P_w^o = a_{w,L} P_w^o \quad (\text{Eq. VIII.28})$$

$$P_{E,L} = \gamma_E(x_{E,L}, T)x_{E,L} P_E^o = a_{E,L} P_E^o \quad (\text{Eq. VIII.29})$$

where the activity coefficients in the liquid feed,  $\gamma_i$  [-], have been estimated by the UNIFAC method (*Reid et al., 1987*). Moreover, in the present formulation, mass transfer across the zeolite layer is assumed to be rate limiting, that is, the contribution of the support to the overall mass transfer in the whole membrane (support + zeolite layer) is neglected (i.e.  $P_{v,i}^S \rightarrow P_{v,i}$ ). This simplification seems reasonable, since a maximum contribution of the support to the overall mass transfer up to 5% was found in the present study for VPV data obtained for membrane ZA2 (see also section VI.2.2).

### VIII.2.2.2. Weak confined MS surface diffusivities

For weak confined MS surface diffusivities,  $\mathfrak{D}_i^S(\theta_v) = \mathfrak{D}_i^S(0)$ . Therefore, the set of Eqs. VIII.24 and VIII.25 is transformed into Eqs. VIII.30 and VIII.31, respectively, for water and ethanol

$$N_w^S = -\rho_s q_M M_w \mathfrak{D}_w^S(0) \frac{\nabla \theta_w}{(1 - \theta_w)} \quad [\text{kg m}^{-2} \text{s}^{-1}] \quad (\text{Eq. VIII.30})$$

$$N_E^S = -\rho_s q_M M_E \mathfrak{D}_E^S(0) \left[ \nabla \theta_E + \theta_E \frac{\nabla \theta_w}{(1 - \theta_w)} \right] \quad [\text{kg m}^{-2} \text{s}^{-1}], \quad (\text{Eq. VIII.31})$$

The resolution of Eqs. VIII.30 and VIII.31 allow to obtain Eqs. VIII.32 and VIII.33 for surface fluxes

$$N_w^S = \frac{\rho_s q_M M_w \mathfrak{D}_w^S(0)}{\ell_{ZA}} \text{Ln} \left( \frac{1 - \theta_{w,v}}{1 - \theta_{w,L}} \right) \quad (\text{Eq. VIII.32})$$

$$N_E^S = \frac{M_E \mathfrak{D}_E^S(0)}{M_w \mathfrak{D}_w^S(0)} N_w^S \left[ \frac{\theta_{E,v} - \theta_{E,L} \exp \left( \frac{N_w^S \ell_{ZA}}{\rho_s q_M M_w \mathfrak{D}_w^S(0)} \right)}{1 - \exp \left( \frac{N_w^S \ell_{ZA}}{\rho_s q_M M_w \mathfrak{D}_w^S(0)} \right)} \right] \quad (\text{Eq. VIII.33})$$

while the selectivity towards water separation,  $\alpha_{w/E}$  [-], is described by Eq. VIII.34

$$\alpha_{w/E} = \frac{X_E}{X_w} \frac{N_w^S}{N_E^S} = \frac{X_E}{X_w} \frac{M_w}{M_E} \frac{D_w^S(0)}{D_E^S(0)} \left[ \frac{(\theta_{w,L} - \theta_{w,v})}{\theta_{E,L}(1 - \theta_{w,v}) - \theta_{E,v}(1 - \theta_{w,L})} \right] \quad (\text{Eq. VIII.34})$$

It should be stressed that the set of Eqs. VIII.32-VIII.33 is identical to that earlier obtained from the general analytical solution found by *Krishna and Baur (2004)* for a binary system under the same assumptions. Regarding the form of Eq. VIII.33, the ethanol surface flux is coupled to that of water. Transforming fractional occupancies into partial pressures, Eqs. VIII.32 and VIII.33 become Eqs. VIII.35 and VIII.36

$$N_w^S = \frac{\rho_s q_M M_w D_w^S(0)}{\ell_{ZA}} \text{Ln} \left( \frac{1 + K_w^S a_{w,L} P_w^o}{1 + K_w^S P_{w,v}} \right) \quad (\text{Eq. VIII.35})$$

$$N_E^S = \frac{M_E D_E^S(0) K_E^S}{M_w D_w^S(0) K_w^S} \left( \frac{a_{w,L} P_w^o - P_{w,v}}{a_{E,L} P_E^o - P_{E,v}} \right) N_w^S \quad (\text{Eq. VIII.36})$$

### VIII.2.2.3. Strong confined MS surface diffusivities

On the other hand, for strong confined MS surface diffusivities,  $D_i^S(\theta_v) = D_i^S(0) \theta_v$ , and under the same assumptions above aforementioned, the set of Eqs. VIII.24 and VIII.25 is now transformed into Eqs. VIII.37 and VIII.38, respectively, for water and ethanol

$$N_w^S = -\rho_s q_M M_w D_w^S(0) \nabla \theta_w \quad [\text{kg m}^{-2} \text{s}^{-1}] \quad (\text{Eq. VIII.37})$$

$$N_E^S = -\rho_s q_M M_E D_E^S(0) [(1 - \theta_w) \nabla \theta_E + \theta_E \nabla \theta_w] \quad [\text{kg m}^{-2} \text{s}^{-1}], \quad (\text{Eq. VIII.38})$$

The resolution of Eqs. VIII.37 and VIII.38 allows to obtain Eqs. VIII.39 and VIII.40 for surface fluxes

$$N_w^S = \frac{\rho_s q_M M_w D_w^S(0)}{\ell_{ZA}} (\theta_{w,L} - \theta_{w,v}) \quad (\text{Eq. VIII.39})$$

$$N_E^S = \frac{\rho_s q_M M_E D_E^S(0)}{\ell_{ZA}} (1 - \theta_{w,L}) (\theta_{E,L} - \theta_{E,v}) + \frac{M_E D_E^S(0)}{M_w D_w^S(0)} \theta_{E,L} N_w^S \quad (\text{Eq. VIII.40})$$

while the selectivity towards water separation,  $\alpha_{w/E}$  [-], is described by Eq. VIII.41

$$\alpha_{w/E} = \frac{X_E}{X_w} \frac{N_w^S}{N_E^S} = \frac{X_E}{X_w} \frac{M_w}{M_E} \frac{D_w^S(0)}{D_E^S(0)} \left[ \frac{(\theta_{w,L} - \theta_{w,v})}{\theta_{E,L}(1 - \theta_{w,v}) - \theta_{E,v}(1 - \theta_{w,L})} \right] \quad (\text{Eq. VIII.41})$$

Again, the set of Eqs. VIII.37-VIII.38 is identical to that earlier obtained from the general analytical solution found by *Krishna and Baur (2004)* for a binary system under the same assumptions. Interestingly, the final equation obtained for the selectivity for both weak and strong confined MS surface diffusivities, Eqs. VIII.34 and VIII.41, respectively, are identical. Furthermore, the form of Eq. VIII.39 is identical to the **adsorption-diffusion model** used by *Shah et al. (2000)* to describe the VPV of pure water through composite zeolite NaA membranes, and the ethanol surface flux is coupled to water surface flux (second term on the right-hand of Eq. VIII.40). Transforming fractional occupancies into partial pressures, Eqs. VIII.39 and VIII.40 become Eqs. VIII.42 and VIII.43

$$N_w^S = \frac{\rho_S q_M M_w \mathcal{D}_w^S(0) K_w^S P_w^o}{\ell_{ZA}} \left( \frac{a_{w,L}}{1 + K_w^S a_{w,L} P_w^o} - \frac{P_{w,v}/P_w^o}{1 + K_w^S P_{w,v}^o} \right) \quad (\text{Eq. VIII.42})$$

$$N_E^S = \frac{\rho_S q_M M_E \mathcal{D}_E^S(0)}{\ell_{ZA}} \left( \frac{1 + K_{E,L}^S a_{E,L} P_E^o}{1 + K_w^S a_{w,L} P_w^o} \right) \left( \frac{K_{E,L}^S a_{E,L} P_E^o}{1 + K_w^S a_{w,L} P_w^o} - \frac{P_{E,v}}{1 + K_w^S P_{w,v}^o} \right) + \frac{K_E^S a_{E,L} P_w^o}{(1 + K_w^S a_{w,L} P_w^o)} \frac{M_E \mathcal{D}_E^S(0)}{M_w \mathcal{D}_w^S(0)} N_w^S \quad (\text{Eq. VIII.43})$$

It should be noted that the mathematical form of Eq. VIII.42 indicates that water might permeate according to a pseudo-fickian process. Moreover, Eq. VIII.42 allows the definition of a water permeability,  $Q_w^S$  [ $\text{kg m}^{-1} \text{h}^{-1}$ ], which can include three contributions to water mass transfer in the PV process: (1) MS surface diffusivity of water at zero coverage, (2) water adsorption constant, and (3) saturation vapor pressure of water, that is

$$Q_w^S = \rho_S q_M M_w \mathcal{D}_w^S(0) K_w^S P_w^o \quad (\text{Eq. VIII.44})$$

Since all these contributions to water permeability are temperature-dependent,  $Q_w^S$  can be wholly regarded as an activated process, in agreement with the trends shown in Figure V.5

$$Q_w^S = \rho_S q_M M_w \mathcal{D}_w^S(0) K_w^S P_w^o = A_{w,\text{eff}}^S \exp\left(\frac{-E_{w,\text{eff}}^S}{RT}\right), \quad (\text{Eq. VIII.45})$$

where  $E_{w,\text{eff}}^S$  and  $A_{w,\text{eff}}^S$  are regarded, respectively, as an effective activation energy [ $\text{kJ mol}^{-1}$ ] and a pre-exponential factor [ $\text{kg m}^{-1} \text{h}^{-1}$ ]. According to Eq. VIII.45, both parameters might include three contributions related to surface diffusion, adsorption and vaporization as it is outlined in Eqs. VIII.46 and VIII.47

$$E_{w,\text{eff}}^S = E_w^S + \Delta H_w^o + R A \quad (\text{Eq. VIII.46})$$

$$A_{w,\text{eff}}^S = \rho_S q_M M_w A_w^S \exp\left(\frac{\Delta S_w^0}{R}\right) \exp(B), \quad (\text{Eq. VIII.47})$$

where parameters **A** and **B** belong to the Antoine Equation ( $\ln(P_w^0) = B - A/T$ ), which accounts for the evolution of saturation vapor pressure with the temperature. For water in the temperature range 293-363 K,  $A = 5300 \text{ K}^{-1}$  and  $B = 20.95 [-]$ .

#### VIII.2.2.4. Fitting of experimental water and ethanol surface flux data

A least-square non-linear optimization method, based on the Levenberg-Marquardt algorithm, was used to adjust the parameters of the models by comparison of predicted and experimental water and ethanol surface fluxes for membrane ZA2, for which a higher number of VPV experiments were performed. In the fitting process, MS surface diffusivities at zero loading and the adsorption constants were expressed by Eqs. VIII.48 and VIII.49

$$D_i^S(0)(T) = D_i^S(0)(T_M) \exp\left[\frac{-E_i^S}{R} \left(\frac{1}{T} - \frac{1}{T_M}\right)\right] \quad i = W, E \quad (\text{Eq. VIII.48})$$

$$K_i^S(T) = K_i^S(T_M) \exp\left[\frac{-\Delta H_i^0}{R} \left(\frac{1}{T} - \frac{1}{T_M}\right)\right], \quad (\text{Eq. VIII.49})$$

where  $T_M$  is the mean temperature [K] of the experimental series. The fitting process was done in two subsequent steps. Firstly, water parameters were adjusted by fitting experimental water fluxes to Eqs. VIII.35 and VIII.42, respectively, for weak and strong confined MS surface diffusivities. Subsequently, ethanol parameters were adjusted by fitting experimental ethanol fluxes to Eq. VIII.36 and VIII.43, respectively, for both confinements.

#### VIII.2.2.5. Correlations for surface fluxes and selectivities for membrane ZA2

Figures VIII.5a-b compare both the experimental water and ethanol fluxes obtained in the VPV conditions indicated in Table VIII.3 to fluxes adjusted to Eqs. VIII.35 and VIII.36, respectively, for weak confined MS surface diffusivities and to Eqs. VIII.42 and VIII.43 for strong confined MS surface diffusivities. For strong confined MS surface diffusivities, excellent fittings are obtained for both water and ethanol fluxes, while for weak MS surface diffusivities, only good fittings are obtained for water fluxes. For ethanol, no convergence of Eq. VIII.43 to the experimental ethanol fluxes data was obtained. Therefore, the adsorption-diffusion model derived from MS strong confined diffusivities (see section VIII.2.2.3) seems to provide a better description of the VPV process for the separation of ethanol/water mixtures by zeolite NaA membranes. Moreover, for strong confinement, the experimental selectivities

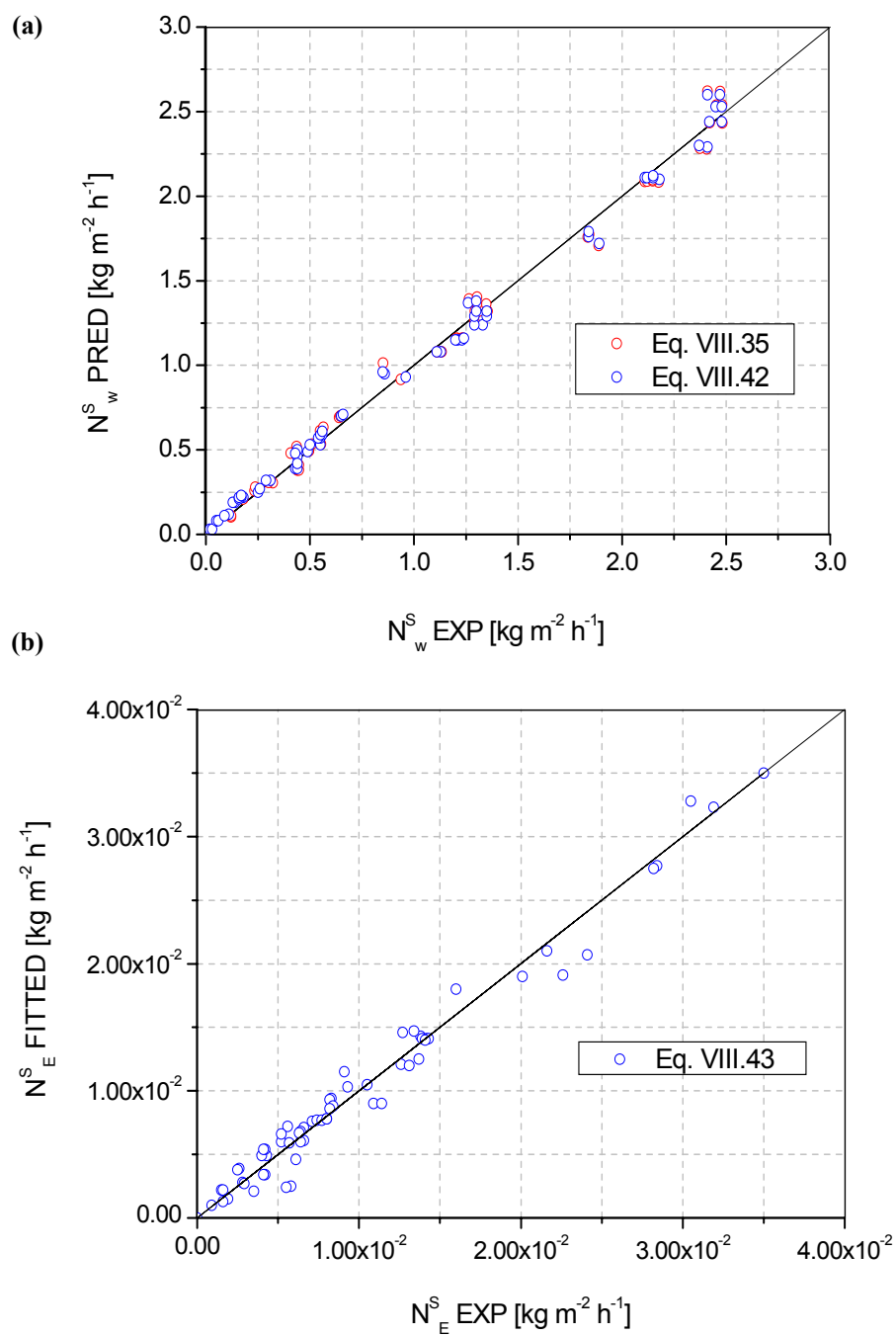


**Figure VIII.5:** Comparison between experimental and fitted trends for (a) water flux, (b) ethanol flux for membrane ZA2 for weak and strong confined MS surface diffusivities. No convergence is observed for ethanol fluxes for the former diffusivities. Experimental conditions as in Table VIII.3.

also agree fairly well with the values predicted by the model (see Figure VIII.6). The statistics of the fittings and the fitted parameters are summarized, respectively, in Tables VIII.4 and VIII.5. The adsorption constants and MS surface diffusivities at zero coverage for both water and ethanol for strong confined diffusivities are described, respectively, by Eqs. VIII.50 – VIII.53 and by Eqs. VIII.37 – VIII.38

$$K_w^S(T) = (0.11 \pm 0.03) \exp \left[ \frac{(43 \pm 6)1000}{8.314} \left( \frac{1}{T} - \frac{1}{333.1} \right) \right] \text{ [kPa}^{-1}] \quad (\text{Eq. VIII.50})$$

$$D_w^S(T) = (2.97 \pm 0.40)10^{-11} \exp \left[ - \frac{(35 \pm 5)1000}{8.314} \left( \frac{1}{T} - \frac{1}{333.1} \right) \right] \text{ [m}^2 \text{ s}^{-1}] \quad (\text{Eq. VIII.51})$$

$$K_E^S(T) = (1.17 \pm 0.37)10^{-2} \exp \left[ \frac{(37 \pm 8)1000}{8.314} \left( \frac{1}{T} - \frac{1}{333.1} \right) \right] \text{ [kPa}^{-1}] \quad (\text{Eq. VIII.52})$$

$$D_E^S(T) = (1.17 \pm 0.31)10^{-12} \exp \left[ \frac{(23 \pm 6)1000}{8.314} \left( \frac{1}{T} - \frac{1}{333.1} \right) \right] \text{ [m}^2 \text{ s}^{-1}] \quad (\text{Eq. VIII.53})$$

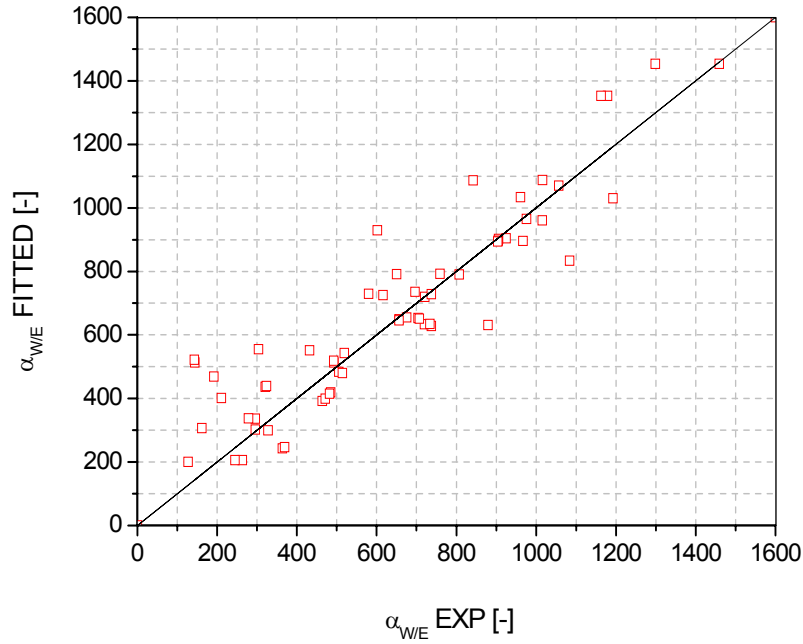


**Figure VIII.6:** Comparison between experimental and fitted trends for water/ethanol selectivity for strong confined MS surface diffusivities for membrane ZA2. Experimental conditions as in Table VIII.3.

**Table VIII.4:** Results of the fittings

Species	Weak confined MS diffusivities		Strong confined MS diffusivities	
	SQ [(kg m <sup>-2</sup> h <sup>-1</sup> ) <sup>2</sup> ]	Coef. Correlation (r <sup>2</sup> )	SQ [(kg m <sup>-2</sup> h <sup>-1</sup> ) <sup>2</sup> ]	Coef. Correlation (r <sup>2</sup> )
Water	7.46 × 10 <sup>-2</sup>	0.9973	6.11 × 10 <sup>-2</sup>	0.9976
Ethanol	No convergence	No convergence	1.06 × 10 <sup>-4</sup>	0.9886

**Table VIII.5:** Parameters fitted the models for membrane ZA2.

Species	Parameter	Adjusted values for weak confined MS diffusivities *	Adjusted values for strong confined MS diffusivities *
Water	$\Delta H_w^o$ [kJ mol <sup>-1</sup> ]	-33 ± 23	-43 ± 6
	$K_w^S(T_M)$ [kPa <sup>-1</sup> ]	0.31 ± 0.19	0.11 ± 0.03
	$E_w^S$ [kJ mol <sup>-1</sup> ]	30 ± 11	35 ± 5
	$D_w^S(0)(T_M)$ [m <sup>2</sup> s <sup>-1</sup> ]	(1.03 ± 0.31) × 10 <sup>-11</sup>	(2.97 ± 0.37) × 10 <sup>-11</sup>
Ethanol	$\Delta H_E^o$ [kJ mol <sup>-1</sup> ]	No convergence	-37 ± 8
	$K_E^S(T_M)$ [kPa <sup>-1</sup> ]	No convergence	(1.17 ± 0.37) × 10 <sup>-2</sup>
	$E_E^S$ [kJ mol <sup>-1</sup> ]	No convergence	23 ± 6
	$D_E^S(0)(T_M)$ [m <sup>2</sup> s <sup>-1</sup> ]	No convergence	(1.17 ± 0.31) × 10 <sup>-12</sup>

\* Confidence interval for a probability level of 95%

On the other hand, experimental and fitted trends for both water and ethanol fluxes with feed weight composition are depicted, respectively, in Figures VIII.7a-b. As was aforementioned in section V.1.3, water surface flux is not altered by the presence of ethanol, except for low water activities. However, the ethanol flux is strongly reduced by the presence of water in the liquid feed. This latter trend might be ascribed to the reduction of selectivity with the feed composition for water fractions higher than 20 mol% (10 wt.%). The *adsorption-diffusion* model, through the set of Eqs. VIII.42 and VIII.43, reproduce successfully the trends outlined in Figures VIII.7a-b, which confirms the relevant role of water adsorption in the zeolite layer in the PV process, that is, the separation behavior of the membrane seems to be governed by differences in adsorption.



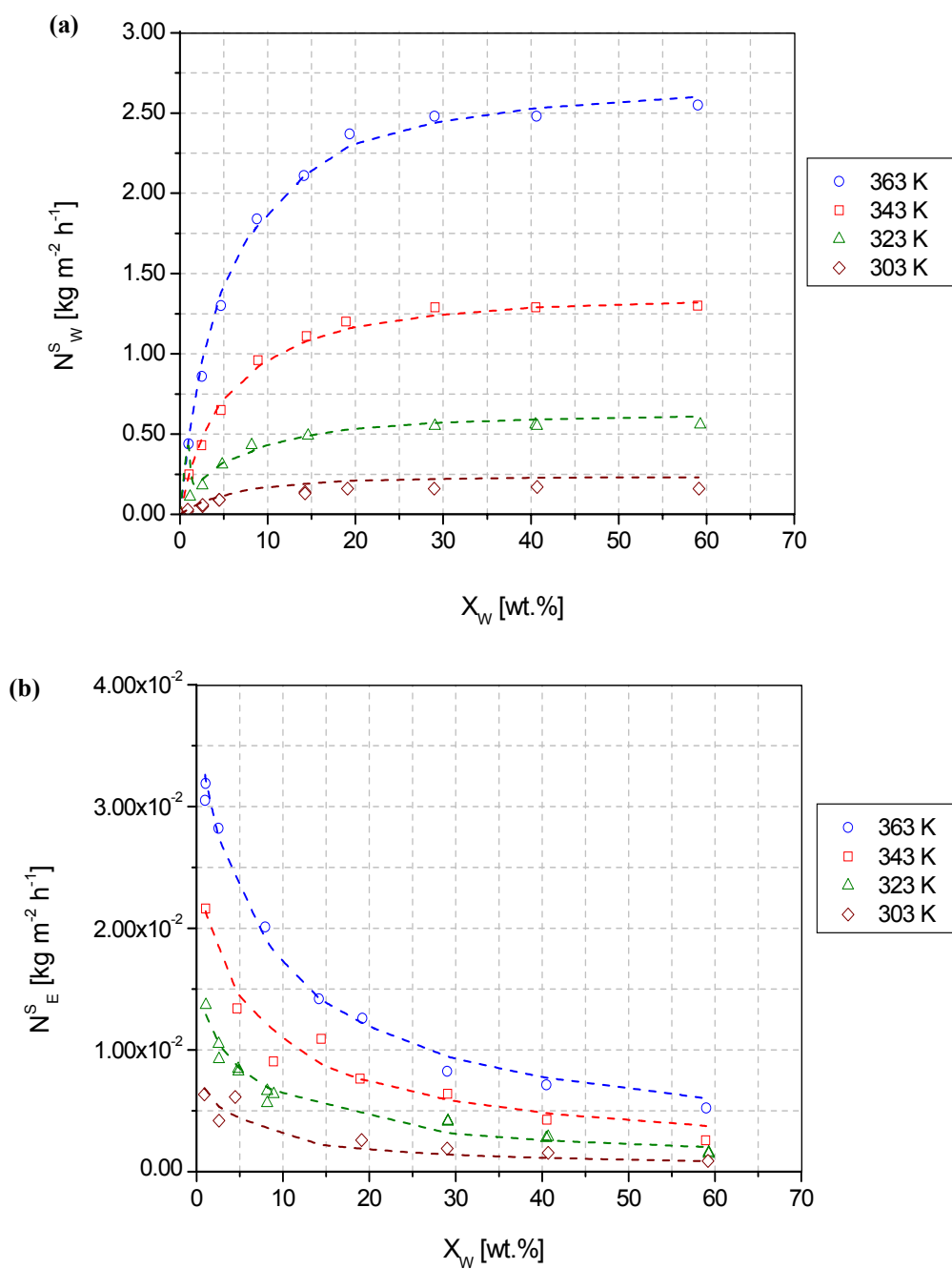


**Figure VIII.7:** Evolution of (a) water flux and (b) ethanol flux with feed weight composition for membrane ZA2. Dashed lines refer to the fittings to the adsorption-diffusion model. Experimental conditions as in Table VIII.3.

### VIII.2.2.6. Adsorption-diffusion vs. Solution-diffusion model

Figure VIII.8 shows the trends for water and ethanol fluxes with the driving force  $\Delta P_1 = a_{i,L} P_1^0 - P_{i,v}$  used for in the *solution-diffusion* model at 363 K (Eq. I.50, see section I.4.3.2). As can be seen, the solution-diffusion model fails to predict the PV behavior in zeolite NaA membranes, because the experimental fluxes do not show a linear trend with the pressure driving force. It should be mentioned that water fluxes show a linear trend with its driving force for  $\Delta P_w$  values comprised between 0-30 kPa (water fractions in the range 0-8.5 wt%, but beyond 30 kPa, important deviations from the linear trend are observed. Moreover, the ethanol flux is far to be predicted by the solution-diffusion model, because no linear trends are observed, even for low values of its driving force. Consequently, in agreement with the general ideas put forward in section I.4.3.2, despite its simplicity and in contrast to the adsorption-diffusion model, Figure VIII.8 confirms that this model does not provide a good basis for the description of mass transfer through zeolite membranes.

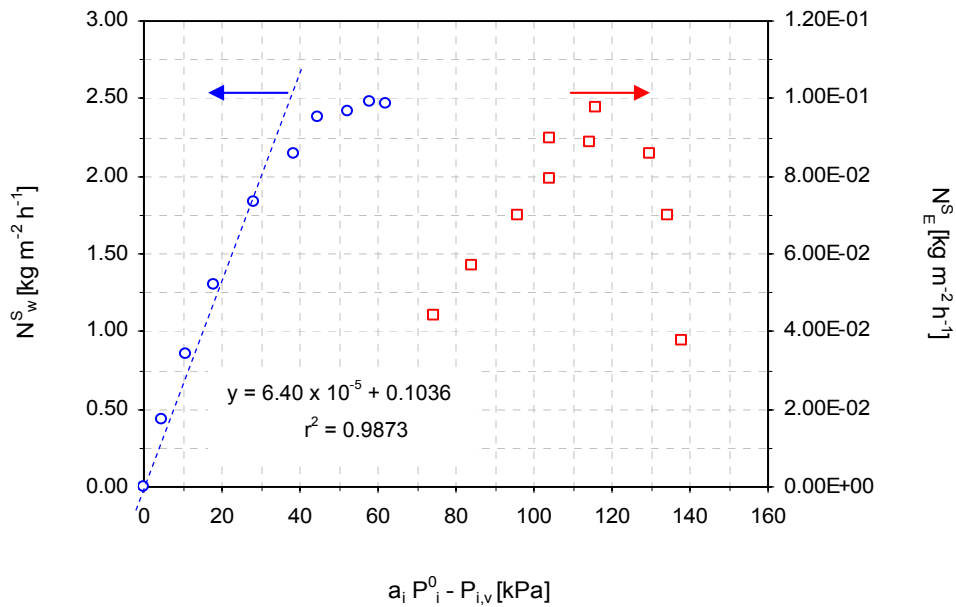


**Figure VIII.8:** Trends for water and ethanol fluxes with the driving force  $\Delta P_1 = a_{i,L} P_1^0 - P_{i,v}$  at 363 K for membrane ZA2.

### VIII.2.2.7. Discussion

In view of the fittings presented in section VIII.2.2.5, the Maxwell-Stefan formalism appears to constitute an excellent basis to account for the PV process of ethanol/water

mixtures through zeolite NaA membranes. Table VIII.6 summarizes the fitted values obtained for the adsorption constants and MS surface diffusivities at zero coverage for water together with some literature data and with the values determined for these parameters, respectively, from adsorption isotherms (see section VII.1) and adsorption kinetics (see section VIII.1) in zeolite NaA powder.

**Table VIII.6:** Adjusted values of adsorption constants and MS surface diffusivities at zero coverage for water for membrane ZA2 and comparison with literature data

<i>Parameter</i>	<i>Value</i>	<i>Method</i>	<i>References</i>
$\Delta H_w^o$ [kJ mol <sup>-1</sup> ]	-45 ± 2	Breakthrough curve <b>VPV in a membrane</b>	<b>Table VII.4 (This study)</b> <b>This study</b>
	-43 ± 6		
$K_w^S$ [kPa <sup>-1</sup> ]	4.7 <sup>(1)</sup>	TEOM	Zhu et al. (2005)
	1.4 ± 0.1 <sup>(1)</sup>	Breakthrough curve <b>VPV in a membrane</b>	<b>Table VII.4 (This study)</b> <b>This study</b>
	0.11 ± 0.03 <sup>(2)</sup>		
$E_w^S$ [kJ mol <sup>-1</sup> ]	58	Water vapor permeance in a membrane	Zhu et al. (2005)
	34 ± 2	Breakthrough curve <b>VPV in a membrane</b>	<b>Eq. VIII.16 (This study)</b> <b>This study</b>
	35 ± 5		
$D_w^S(0)$ [m <sup>2</sup> s <sup>-1</sup> ]	10 <sup>-9</sup> - 10 <sup>-10</sup> <sup>(2,3)</sup>	QENS / PFG RMN <sup>(4)</sup> VPV in a membrane	Paoli et al. (2002) Shah et al. (2000)
	3.0-5.0 × 10 <sup>-12</sup> <sup>(2)</sup>		
	(1.94 ± 0.15) × 10 <sup>-16</sup> <sup>(2)</sup>	Breakthrough curve <b>VPV in a membrane</b>	<b>Eq. VIII.16 (This study)</b> <b>This study</b>
	(2.97 ± 0.37) × 10 <sup>-11</sup> <sup>(2)</sup>		

<sup>(1)</sup> Determined at 341 K

<sup>(2)</sup> Determined at 298-333 K

<sup>(3)</sup> Self-diffusivity of water in zeolite A at 378 K for 20 molecules per  $\alpha$ -cage

<sup>(4)</sup> QENS: Quasi-elastic neutron scattering  
PFG RMN: Pulse field gradient NMR

In light of the data exposed in Tables VIII.5 and VIII.6, the computed value for the adsorption enthalpy of water,  $-43.1 \pm 6$  kJ mol<sup>-1</sup>, is of the same order of magnitude as that found in the unary adsorption experiments of water in zeolite NaA powder (see section VII.1). Moreover, the fitted value for the adsorption constant for water at  $T_M = 333$  K,  $0.11 \pm 0.03$  kPa<sup>-1</sup>, is one order of magnitude lower to that found in this work for water adsorption on zeolite NaA powder (see Table VII.7). The lower value found in this work might be ascribed to the contribution of non-zeolite pores, which might involve less adsorption strength for water than zeolite pores. In addition, the adsorption constant for water at  $T_M$  is one order of magnitude higher than that of ethanol ( $0.11 \pm 0.03$  vs.  $(1.17 \pm 0.37) \times 10^{-2}$  kPa<sup>-1</sup>), thus confirming the simplification  $q_w \gg q_E$  done in the derivation of Eqs. VIII.24 and VIII.25. Regarding the values of the activation energy and enthalpy of adsorption for water, the

computed value of its effective activation energy is  $+36 \text{ kJ mol}^{-1}$ , which is in fairly good agreement with the value determined listed in Table V.2 for membrane ZA2.

The diffusivity values for both water and ethanol at zero coverage show values of  $(2.97 \pm 0.37) \times 10^{-11}$  and  $(1.17 \pm 0.31) \times 10^{-12} \text{ m}^2 \text{ s}^{-1}$ , respectively (see Table VIII.5). The former is in quite good agreement with the value reported by *Shah et al. (2000)*,  $3.0\text{-}5.0 \times 10^{-12} \text{ m}^2 \text{ s}^{-1}$ , computed from the PV of pure water through a commercial zeolite NaA membrane. The diffusivity of ethanol at zero coverage is one order of magnitude lower than that of water. This result is consistent with the differences in the kinetic diameters of both molecules (0.29 vs. 0.43 nm). However, the experimental values of MS surface diffusivities at zero coverage determined for both water and ethanol are ca. 5 orders of magnitude higher than those determined from adsorption kinetics (see section VIII.1). Invalid assumptions made in analysis of macroscopic data (*Kapteijn et al., 1995*), differences in the interpretation of equilibrium vs. non-equilibrium measurements (*Jobic et al., 1999*), and the inaccuracy of each technique when applied near its limits (*Sun et al., 1996*) are among the reasons suggested for these large differences. Furthermore, this discrepancy might also provide evidence of a certain role of *intercrystalline* pathways or non-zeolite pores, that is grain boundaries and meso- and macroporous defects, in the overall mass transfer through the zeolite NaA layers. Furthermore, the apparent values of MS surface diffusivities of water found in this work approach the range values of self-diffusivities determined by *Paoli et al. (2002)* by the QENS and PFG-NMR techniques. The contribution of large defects might be also responsible for the higher values observed for MS surface diffusivities of ethanol,  $(1.17 \pm 0.31) \times 10^{-12} \text{ m}^2 \text{ s}^{-1}$ , compared to those determined from adsorption kinetics,  $(5.99 \pm 1.41) \times 10^{-16} \text{ m}^2 \text{ s}^{-1}$ .

On the other hand, although the activation energy for the surface diffusion of ethanol is expected to be much higher than that of water due to the higher kinetic diameter of the former, the values found from the fittings are quite similar (see Table VIII.5). It should be noted that the activation energy for water found in this study,  $35 \pm 5 \text{ kJ mol}^{-1}$ , is in agreement with the value found from adsorption kinetics,  $34 \pm 2 \text{ kJ mol}^{-1}$ , and in of the same order as the value of  $58 \text{ kJ mol}^{-1}$  reported by *Zhu et al. (2005)*. However, the activation energy for ethanol,  $23 \pm 6 \text{ kJ mol}^{-1}$ , is much lower than the value that would be expected. This lower value for ethanol activation energy might provide additional evidence of the contribution of mass transfer through *grain boundaries* and large defects on the fitted parameters.

The VPV performance of zeolite NaA membranes towards the separation of ethanol/water mixtures is strongly dependent on feed composition and temperature. The adsorption-diffusion model developed in this section with the set of assumptions and constraints put forward in section VIII.2.2.1 provides a good basis for the description of the PV process through zeolite NaA membranes and reveals a good tool for practical applications. However, to improve the level of description of the PV process, section VIII.2.3 shows a

modified version of the model, where the binary adsorption equilibrium of water and ethanol in the zeolite NaA layer is modeled by the PRAS theory instead of the Extended Langmuir isotherm, which also includes the contribution of meso- and macroporous defects.

### VIII.2.3. PRAST approach + contribution of large defects

Although the *adsorption-diffusion* model presented in section VIII.2.2, derived from the assumption of strong confined diffusivities, seems to provide a good basis for modeling the VPV dehydration of ethanol/water mixtures by zeolite NaA membranes, as was aforementioned, it lacks of thermodynamic consistency on the basis on the inequality of the molar saturation loadings of both water and ethanol (11.4 vs. 3.5 mol kg<sup>-1</sup>, respectively). To overcome this shortcoming, this section presents an improved version of the adsorption-solution model, where mixture adsorption is described by means of the Predictive Adsorbed Solution Theory (PRAST) that reveals useful for predicting mixture adsorption of water and ethanol vapors in zeolite NaA powder from unary adsorption data (see section VII.1.3). Moreover, the contribution of meso- and macroporous defects on the dehydration performance of composite zeolite NaA membranes determined following the general ideas put forward in section VI.2 is also included in the present description.

#### VIII.2.3.1. Modeling binary adsorption equilibria of water and ethanol

The same concepts outlined in section VII.1.3 for modeling the binary adsorption equilibrium of water and ethanol vapors in zeolite NaA powder are extended in this section to account for the binary adsorption equilibrium of both species in the zeolite NaA layers, in a similar way as was previously reported by *Kapteijn et al. (2000)* for modeling mass transfer of gas mixtures through MFI membranes. Using the PRAS theory together with the single-site Langmuir isotherm to model unary adsorption equilibrium, the mixture adsorption of both species is accounted for by solving the set of Eqs. VIII.54 for the zeolite layer (Eq. I.30)

$$P y_i = P_i^{\circ}(\Phi) \gamma_i(\Phi) x_i \quad i = w, E \quad (\text{Eqs. VIII.54})$$

$$\sum_{i=1}^N y_i = \sum_{i=1}^N x_i = 1$$

$$-\frac{\Phi}{RT} = \int_0^{P^{\circ}(\Phi)} \frac{q_i^{\circ}(P_i)}{P_i} \delta P_i = q_{M,i} \text{Ln}(1 + K_i P_i^{\circ}) \geq 0$$

where  $y_i$  and  $x_i$  are the molar fractions of species  $i$  in gas and adsorbate phases [-], respectively,  $\gamma_i(\Phi)$  is the activity coefficient of species  $i$  in the adsorbate [-] (that can be calculated by the recipe provided Appendix C),  $P$  is the total pressure in the gas phase [kPa],

and  $P_i^0(\Phi)$  is the adsorptive saturation pressure corresponding to the solution temperature and surface potential  $\Phi$ . Moreover, the total loading and the loading of each species can be determined, respectively, by Eqs. VIII.55 (Eqs. I.31-I.32) and VIII.56

$$\frac{1}{q^T} = \sum_{i=1}^N \frac{x_i}{q_i^0(\Phi)} \quad [\text{kg mol}^{-1}] \quad (\text{Eq. VIII.55})$$

$$q_i = x_i q^T \quad [\text{mol kg}^{-1}] \quad (\text{Eq. VIII.56})$$

where  $q^T$  is the total amount adsorbed and  $q_i^0(\Phi)$  is the amount of pure species  $i$  adsorbed at surface potential  $\Phi$  [ $\text{J kg}^{-1}$ ]. In comparison to Eq. I.31, the second term on the right-hand that includes the expression  $[\partial \ln \gamma_i(\Phi) / \partial \Phi]_{T,x_i}$  has been removed, because its contribution was found to be  $<5\%$ . Furthermore, the molar saturation loading for the mixture is regarded to depend on the adsorbate composition by Eq. VIII.57

$$\frac{1}{q_M} = \sum_{i=1}^N \frac{x_i}{q_{M,i}} \quad [\text{kg mol}^{-1}] \quad (\text{Eq. VIII.57})$$

### VIII.2.3.2. Equations for surface diffusion

The GMS equations (Eq. VIII.18) constitute again the essential tool to model mass transfer through zeolite NaA layers (including both zeolite pores and grain boundaries) in the PV process for the dehydration of ethanol/water mixtures in the absence of contribution of counterexchange mobility of the adsorbed molecules. Eq. VIII.18 can be complemented with Eq. VIII.23 to account for the contribution of the porous support on the overall mass transfer. In the present formulation, Eq. VIII.18 can be simplified using partial pressures in the zeolite layer instead of molar loadings to account for the surface diffusion of adsorbed species through the use of the condition

$$\sum_{j=1}^N \frac{q_j}{P_i} \frac{\partial P_i}{\partial q_j} \nabla q_j = \frac{q_i}{P_i} \nabla P_i, \quad (\text{Eq. VIII.58})$$

which allows to transform Eq. VIII.18 into Eq. VIII.59

$$N_i^S = -\rho_p D_i^S \frac{q_i}{P_i} \nabla P_i \quad [\text{mol m}^{-2} \text{s}^{-1}] \quad (\text{Eq. VIII.59})$$

Moreover, assuming that mass transfer only takes place along the  $z$ -direction perpendicular to the membrane plane and that zeolite and non-zeolite pores (grain boundaries) are non-tortuous, the pressure gradient in Eq. VIII.59 can be approached to derivatives, that is

$$N_i^S = -\rho_p \mathcal{D}_i^S \frac{q_i}{P_i} \frac{\delta P_i}{\delta z} \quad (\text{Eq. VIII.60})$$

with the boundary conditions:

$$z=0, \quad \rightarrow \quad P_w = P_{w,L}, \quad P_E = P_{E,L}$$

$$z = \ell_{ZA} \rightarrow \quad P_w = P_{w,v}^S, \quad P_E = P_{E,v}^S$$

The pressure of each species at the liquid feed/membrane surface can be calculated by Eqs. VIII.61 and VIII.62 by assuming again vapor-liquid equilibrium

$$P_{w,L} = \gamma_w(x_{w,L}, T) x_{w,L} P_w^o = a_{w,L} P_w^o \quad (\text{Eq. VIII.61})$$

$$P_{E,L} = \gamma_E(x_{E,L}, T) x_{E,L} P_E^o = a_{E,L} P_E^o \quad (\text{Eq. VIII.62})$$

where the activity coefficients in the liquid feed,  $\gamma_i$  [-], have been estimated by the UNIFAC method. Again, the MS surface diffusivities have been selected to depend on the total molar loading,  $q^T$  [mol kg<sup>-1</sup>], for weak and strong confinement

$$\mathcal{D}_i^S(q^T) = \mathcal{D}_i^S(0) \quad (\text{Eq. VIII.63})$$

$$\mathcal{D}_i^S(q^T) = \mathcal{D}_i^S(0) \left( 1 - \frac{q^T}{q_M} \right), \quad (\text{Eq. VIII.64})$$

where  $q_M$  is the molar saturation loading that can be calculated by Eq. VIII.57. Eqs. VIII.63 and VIII.64 can be rewritten to Eq. VIII.65

$$\mathcal{D}_i^S(q^T) = \mathcal{D}_i^S(0) f(q^T), \quad (\text{Eq. VIII.65})$$

Finally, combining Eq. VIII.60 and Eq. VIII.65, the final expression that accounts for surface diffusion in the zeolite NaA layer becomes Eqs. VIII.66 and VIII.67 for water and ethanol, respectively

$$\alpha_w = -\frac{q_w}{q_{M,w}} \frac{f(q^T)}{P_w} \frac{\delta P_w}{\delta \eta} \quad \text{and} \quad \alpha_E = -\frac{q_E}{q_{M,E}} \frac{f(q^T)}{P_E} \frac{\delta P_E}{\delta \eta} \quad (\text{Eqs. VIII.66-VIII.67})$$

where  $\alpha_w$  and  $\alpha_E$  are the dimensionless fluxes of water and ethanol that are defined, respectively, by Eqs. VIII.26 and VIII.27, and  $\eta = z/\ell_{ZA}$  is the dimensionless  $z$ -position in the zeolite layer [-].

The contribution of large meso- and macroporous defects (“intercrystalline porosity”) to the overall mass transfer can be taken into account using the characterization method presented in section VI.2. To this end, the contribution of large defects was subtracted from

the total flux to obtain the contribution of surface flux, which is further modeled by Eqs. VIII.66 and VIII.67. For further details see section VI.2.2.

### VIII.2.3.3. Resolution of the model and fittings to experimental data

Eqs. VIII.66 and VIII.67 were discretized by approximating derivatives to finite differences, thus obtaining the resolution scheme shown in Appendix G for the calculation of the dimensionless fluxes as a function of temperature and feed composition. The relevant data used in the fittings can be found in Table VIII.7 (or VII.9). It should be emphasized that, in the present formulation, the adsorption constants are introduced in the model as input data, whose values correspond to those determined from experimental unary adsorption data of water and ethanol vapors in zeolite NaA powder (see section VII.1). For each VPV experiment carried out at a given temperature and feed composition, the dimensionless fluxes of water and ethanol,  $\alpha_w$  and  $\alpha_E$  [-], respectively, were calculated from the set of equations VIII.54-VIII.57 and the discretized Eqs. VIII.66 and VIII.67. An example of the evolution of the molar loading along the dimensionless thickness of zeolite NaA layer,  $\eta$  [-], for given values of feed and permeate partial pressures for both water and ethanol, being the former at equilibrium with the liquid feed, is shown in Figure VIII.9. As can be seen, as expected, the molar loadings tend to decrease with the dimensionless thickness, especially in the last 30% of the layer thickness.

**Table VIII.7:** Input data for the prediction of binary adsorption isotherms by the PRAST model

<i>Single-site unary adsorption data</i>	<i>Value</i>
$q_{M,w}$ [mol kg <sup>-1</sup> ]	11.40
$q_{M,E}$ [mol kg <sup>-1</sup> ]	3.47
$K_w$ [kPa <sup>-1</sup> ]	5.20
$K_E$ [kPa <sup>-1</sup> ]	2.64

After calculation of all the dimensionless fluxes, a least-square non-linear optimization method, based on the Levenberg-Marquardt algorithm, was used to adjust the MS surface diffusivities at zero loading for both weak and strong confinement by comparison of predicted and experimental water and ethanol surface fluxes. In the fitting process, MS surface diffusivities at zero loading were expressed by Eqs. VIII.68



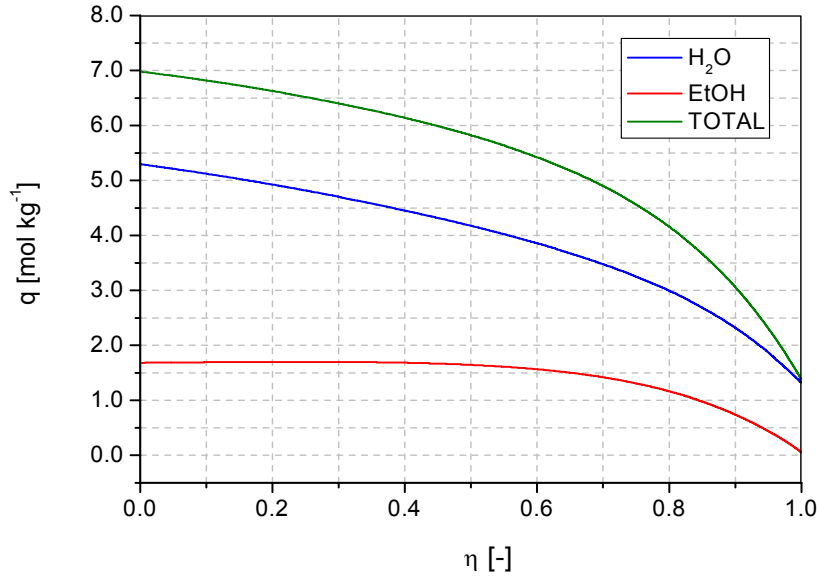


**Figure VIII.9:** Trends for water, ethanol and total loading with the dimensionless thickness of a zeolite NaA layer. Input data:  $T=323$  K;  $a_{w,L} = 0.0653$ ,  $a_{E,L} = 0.9734$ ;  $P_{w,v} = 96.1$  Pa,  $P_{E,v} = 2.6$  Pa. Output data:  $\alpha_w = 1.20$ ,  $\alpha_E = 3.25$ .

$$\mathcal{D}_i(0)(T) = \mathcal{D}_i(0)(T_M) \exp\left[\frac{-E_i^S}{R} \left(\frac{1}{T} - \frac{1}{T_M}\right)\right] \quad i = W, E \quad (\text{Eq. VIII.68})$$

where  $T_M$  is again the mean temperature [K] of the experimental series.

#### VIII.2.3.4. Correlations with experimental data

Figures VIII.10a-b compare both the experimental water and ethanol fluxes obtained for membrane ZA2 in the VPV conditions indicated in Table VIII.3 to the improved model presented in this section, where only one parameter for each surface flux, that is the MS surface diffusivity for the situation of weak confinement, is adjusted. As can be seen, the model predicts successfully the experimental trends observed for both fluxes. The fitted parameters are summarized, respectively, in Table VIII.8. The weak confined MS surface diffusivities at zero coverage for both water and ethanol are described, respectively, by Eqs. VIII.69 – VIII.70

$$\mathcal{D}_w^S(T) = (4.02 \pm 0.26) 10^{-12} \exp\left[-\frac{(34 \pm 2) 1000}{8.314} \left(\frac{1}{T} - \frac{1}{333.1}\right)\right] [\text{m}^2 \text{s}^{-1}] \quad (\text{Eq. VIII.69})$$

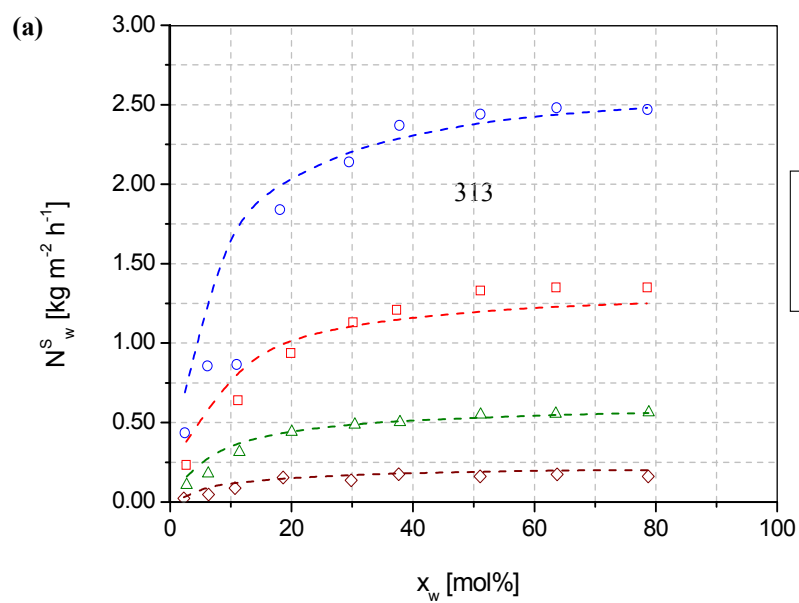
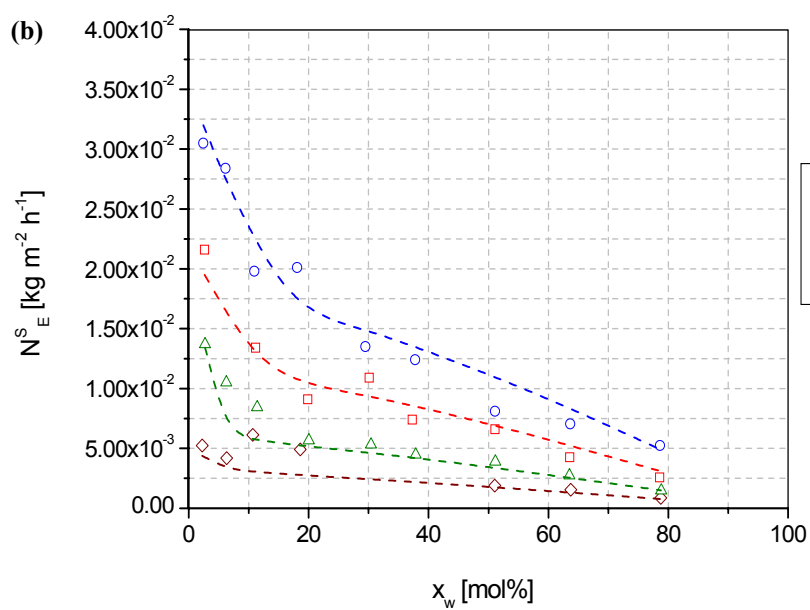


**Figure VIII.10:** Evolution of (a) water flux and (b) ethanol flux with feed molar composition for membrane ZA2. Dashed lines refer to the fittings to the model. Experimental conditions as in Table VIII.3.

**Table VIII.8:** Adjusted values of adsorption constants and MS surface diffusivities at zero coverage for water for membrane ZA2 and comparison with literature data

<i>Parameter</i>	<i>Value</i>	<i>Method</i>	<i>References</i>
$E_w^S$ [kJ mol <sup>-1</sup> ]	34 ± 2 34 ± 6	Breakthrough curve <b>VPV in a membrane</b>	<b>Table VIII.6 (This study)</b> <b>Membrane ZA2 (This study)</b>
$D_w^S(0)$ [m <sup>2</sup> s <sup>-1</sup> ]	10 <sup>-9</sup> - 10 <sup>-10</sup> (1,3) (3.0 ± 5.0) × 10 <sup>-12</sup> (1)	QENS / PFG RMN <sup>(4)</sup> VPV in a membrane	Paoli et al. (2002) Shah et al. (2000)
	(1.33 ± 0.15) × 10 <sup>-16</sup> (2)	Breakthrough curve	<b>Table VIII.6 (This study)</b>
	(2.37 ± 0.26) × 10 <sup>-12</sup> (2)	<b>VPV in a membrane</b>	<b>Membrane ZA1 (This study)</b>
	(2.60 ± 0.26) × 10 <sup>-12</sup> (2)	<b>VPV in a membrane</b>	<b>Membrane ZA2 (This study)</b>
	(4.90 ± 0.26) × 10 <sup>-12</sup> (2)	<b>VPV in a membrane</b>	<b>Membrane ZA3 (This study)</b>
$E_E^S$ [kJ mol <sup>-1</sup> ]	12 ± 5	<b>VPV in a membrane</b>	<b>Membrane ZA2 (This study)</b>
$D_E^S(0)$ [m <sup>2</sup> s <sup>-1</sup> ]	(1.94 ± 0.15) × 10 <sup>-16</sup> (2) (1.29 ± 0.31) × 10 <sup>-13</sup> (2)	Breakthrough curve <b>VPV in a membrane</b>	<b>Eq. VIII.16 (This study)</b> <b>Membrane ZA2 (This study)</b>

<sup>(1)</sup> Determined at 298 K

<sup>(2)</sup> Determined at 323 K

<sup>(3)</sup> Self-diffusivity of water in zeolite A at 378 K for 20 molecules per  $\alpha$ -cage

<sup>(4)</sup> QENS: Quasi-elastic neutron scattering

PFG RMN: Pulse field gradient NMR

$$D_E^S(T) = (1.29 \pm 0.31) 10^{-13} \exp\left[\frac{(12 \pm 5) 1000}{8.314} \left(\frac{1}{T} - \frac{1}{333.1}\right)\right] \text{ [m}^2 \text{ s}^{-1}] \quad (\text{Eq. VIII.70})$$

Furthermore, Figure VIII.11 shows the fittings for a water composition in the feed <20 mol% (10 wt.%) at 323 K for the three membranes whose main characteristics have been outlined in Table VIII.2. As can be seen, the model predicts a similar behavior for all the membranes with fitted weak confined MS surface diffusivities at zero coverage for water that are of the same order (see Table VIII.8). Therefore, the improved model derived for weak confined MS surface diffusivities seems to provide a better description of the PV process for the separation of ethanol/water mixtures in zeolite NaA membranes.

It should be noted that, on the opposite to what was observed in the preliminary fittings presented in section VIII.2.2, weak confined MS surface diffusivities provide better fittings than strong confined MS surface diffusivities with the improved model used in this section. In fact, according to Figure VIII.12, strong confined MS diffusivities do not account for the experimental trends observed for water and ethanol fluxes for membrane ZA2 shown in

Figure VIII.10, which is in agreement with the general trends observed for MS surface diffusivities obtained from breakthrough curve analysis and from weight uptake in the microbalance.

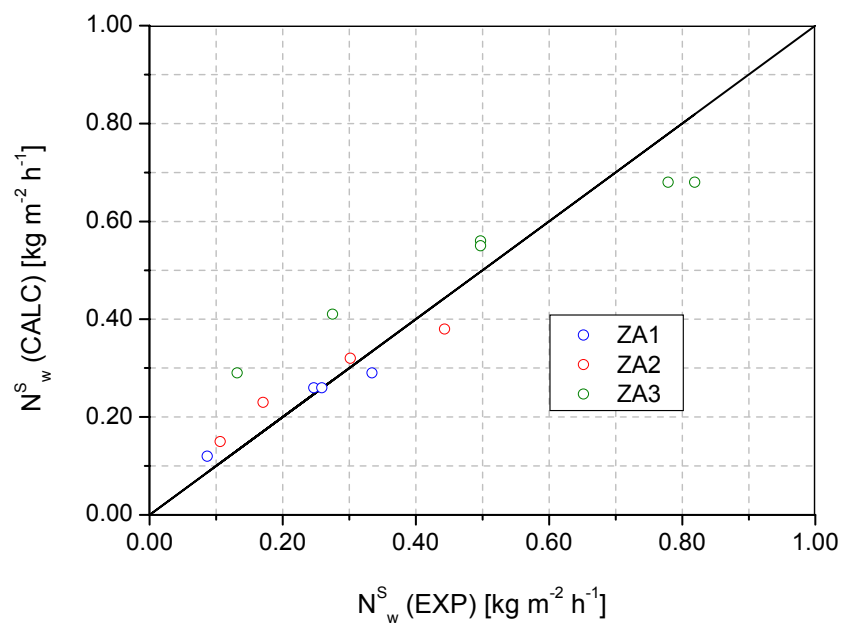


**Figure VIII.11:** Comparison between experimental and fitted trends of water flux for membrane ZA2 under weak confinement. Experimental conditions as in Table VIII.3.

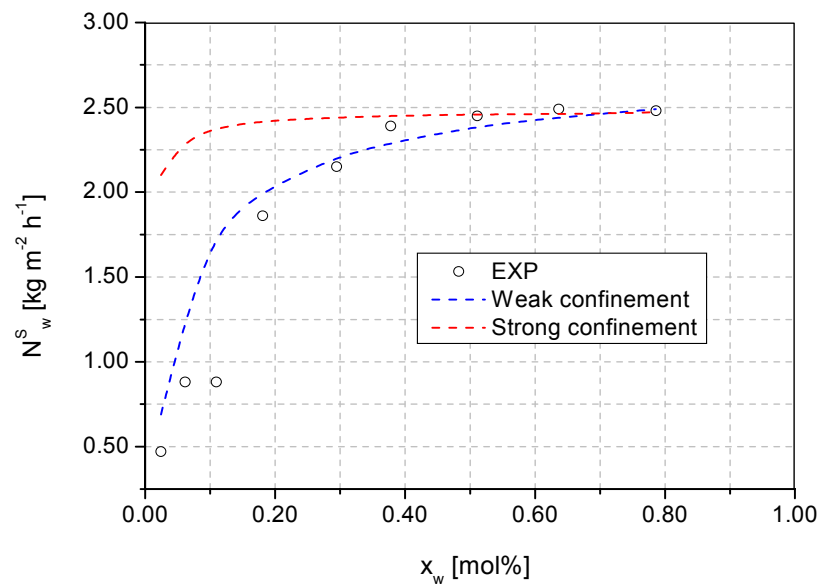


**Figure VIII.12:** Evolution of water flux with feed molar composition at 363 K for membrane ZA2. Dashed lines refer to the fittings to the model for the special cases of weak and strong confined MS surface diffusivities. Experimental conditions as in Table VIII.3.

Finally, the fittings of surface flux data of ethanol deserves special attention. Meanwhile the surface flux of water is practically not affected by the contribution of large pores (contribution <1%), a relevant contribution of the flux through meso- and macropores in the zeolite NaA layer is observed for ethanol, as depicted in Figure VIII.13. This contribution is especially relevant for a water composition in the feed >20 mol% (10 wt.%).

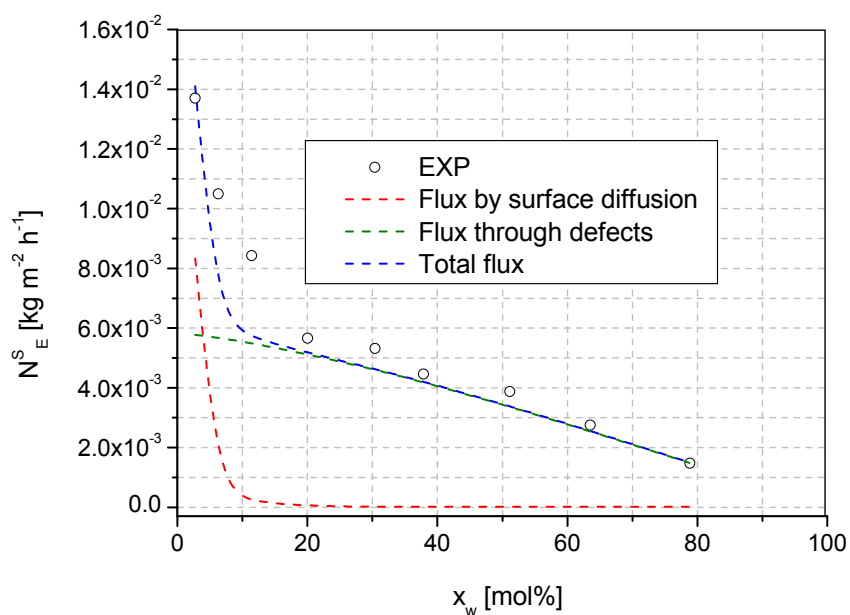


**Figure VIII.13:** Contribution of surface diffusion and flux through large defects on the overall flux of ethanol at 343 K for membrane ZA2.

### VIII.3. DISCUSSION AND FINAL REMARKS: ROLE OF GRAIN BOUNDARIES (NON-ZEOLITE PORES)

In light of the fittings presented in section VIII.2.3.4, the Maxwell-Stefan formalism in its improved version and for weak confinement provides a good description of the PV dehydration ability of zeolite NaA membranes. The fitted values of weak confined MS surface diffusivities at zero coverage at 323 K for both water and ethanol show values in the range  $2.37\text{--}4.90 \times 10^{-12}$  and  $1.94 \times 10^{-13} \text{ m}^2 \text{ s}^{-1}$ , respectively (see Table VIII.7), which are lower than values obtained from the fittings in the preliminary modeling shown in section VIII.2.2. Again, the lower values of MS surface diffusivities at zero coverage of ethanol compared to those of water might be accounted for by the differences in the kinetic diameters of both molecules.

Although the improved model provides MS surface diffusivities that are closer to the experimental values found from breakthrough curve analysis in the differential packed bed and from weight uptake in the microbalance, the former still range over 3-4 orders of magnitude from the latter, which might be again attributed to a role of *intercrystalline* pathways or non-zeolite pores in the overall mass transfer through the zeolite NaA layer.

Among intercrystalline pathways, large defects, namely meso- and macropores, are not expected to be responsible for this apparent lack of consistency, since their contribution was included in the improved model. Therefore, the difference in the order of magnitude of MS surface diffusivities determined from VPV experiments and from breakthrough curve analysis and weight uptake, all macroscopic methods, might be in principle accounted for by grain boundaries of nanoscopic size between adjacent zeolite NaA crystals. Compared to large defects, the flux through which is governed by mechanical fluxes (i.e. pressure-driven viscous and Knudsen fluxes), the flux through grain boundaries is expected to occur by surface diffusion, which might contribute together with zeolite pores to mass transfer. Nevertheless, because grain boundaries are larger in size than zeolite windows, the diffusion through them might be less impelled, that is, they might behave as fast diffusion paths or nanoscopic shortcuts due to anisotropy of the zeolite layers (*Nelson et al., 2001; Philibert, 1991*) (see Figure VIII.14), thus resulting in higher values of apparent MS surface diffusivities.

On the other hand, although the activation energy for the surface diffusion of ethanol is expected to be much higher than that of water due to the higher kinetic diameter of the former, the values found from the fittings with the improved model presented in section VIII.2.3 (see Table VIII.7). It should be noted that the activation energy for water found in the latter study,  $34 \pm 2 \text{ kJ mol}^{-1}$ , is in excellent agreement with the value found from adsorption kinetics,  $34 \pm 2 \text{ kJ mol}^{-1}$ . However, the activation energy for ethanol,  $12 \pm 5 \text{ kJ mol}^{-1}$ , is much lower than that of water, which might provide additional evidence of the contribution of mass transfer through *grain boundaries* on the fitted parameters.

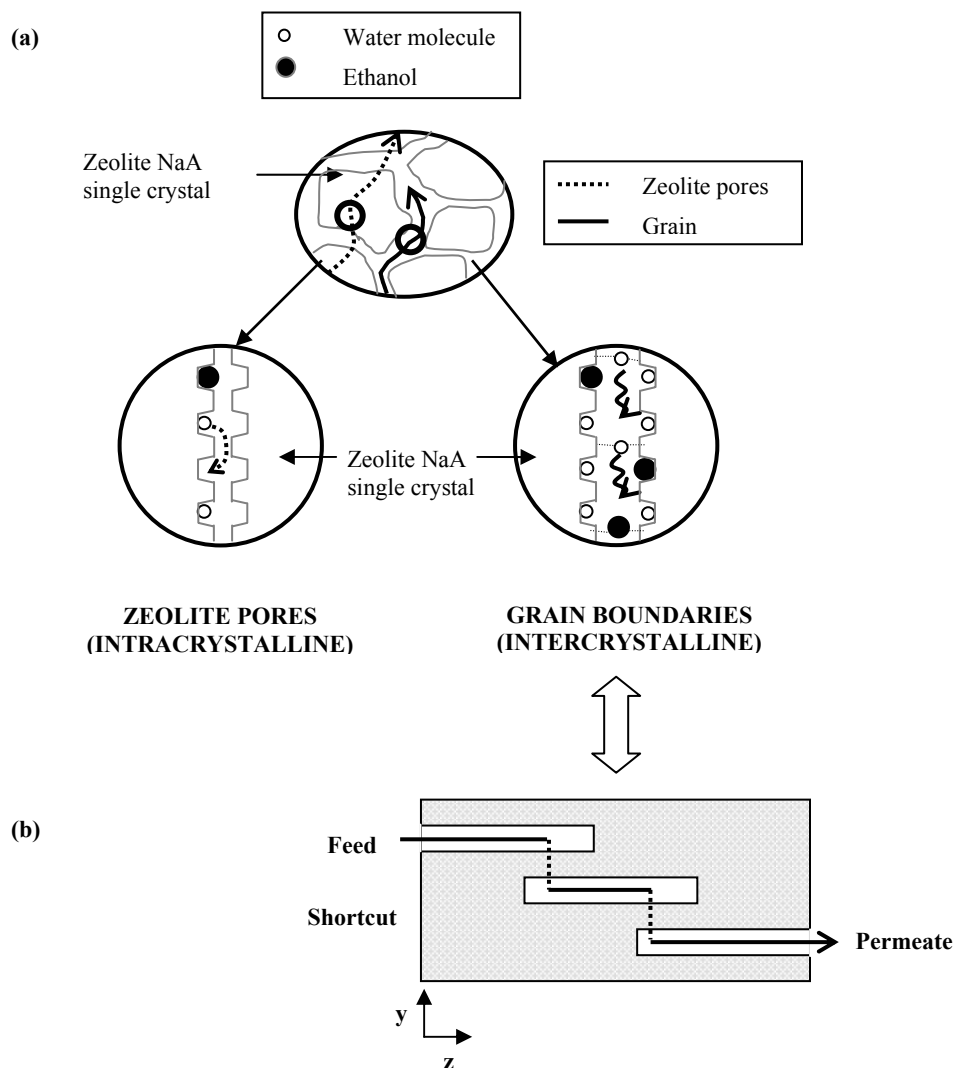


**Figure VIII.14:** Schematic representation of intracrystalline and intercrystalline pathways in the active zeolite NaA layer. (a) Mass transfer through zeolite pores and grain boundaries between adjacent zeolite NaA crystals, and (b) schematic representation of a shortcut through an anisotropic membrane.